Materials Horizons

ROYAL SOCIETY OF CHEMISTRY

REVIEW

View Article Online
View Journal | View Issue

Cite this: *Mater. Horiz.*, 2023, **10**, 2343

Microreactor-based micro/nanomaterials: fabrication, advances, and outlook

Jianfeng Ran,[abc] Xuxu Wang,[abc] Yuanhong Liu,[abc] Shaohua Yin, *[abc] Shiwei Li*[abc] and Libo Zhang*[abc]

Received 4th March 2023,
Accepted 14th April 2023

DOI: 10.1039/d3mh00329a

rsc.li/materials-horizons

Micro/nanomaterials are widely used in optoelectronics, environmental materials, bioimaging, agricultural industries, and drug delivery owing to their marvelous features, such as quantum tunneling, size, surface and boundary, and Coulomb blockade effects. Recently, microreactor technology has opened up broad prospects for green and sustainable chemical synthesis as a powerful tool for process intensification and microscale manipulation. This review focuses on recent progress in the microreactor synthesis of micro/nanomaterials. First, the fabrication and design principles of existing microreactors for producing micro/nanomaterials are summarized and classified. Afterwards, typical examples are shown to demonstrate the fabrication of micro/nanomaterials, including metal nanoparticles, inorganic nonmetallic nanoparticles, organic nanoparticles, Janus particles, and MOFs. Finally, the future research prospects and key issues of microreactor-based micro/nanomaterials are discussed. In short, microreactors provide new ideas and methods for the synthesis of micro/nanomaterials, which have huge potential and inestimable possibilities in large-scale production and scientific research.

Wider impact statement

Micro/nanomaterial processing, which belongs to the manufacturing and application of materials to achieve industrial product design at the micro- or nanoscale, is one of the most interesting industries of the 21st century and is considered to have potential as large as the IT and biotechnology fields. However, the drawback of relative inflexibility in conventional batch-based synthesis methods has led to a growing interest in microfluidic wet-chemical synthesis, which has enabled the development of continuous manufacturing processes. Microreactor technology has opened up broad prospects for green and sustainable chemical syntheses as a powerful tool for process intensification and microscale manipulation. This study summarizes the fabrication and design principles of microreactors and focuses on typical application examples that are widely used in the manufacture of micro/nano materials, including the synthesis of inorganic, organic, and composite micro/nanomaterials. Finally, an outlook is provided for future research prospects and key issues, including the continued optimization of microreactor design and processing costs, integration of multifunctional nanomaterials into microreactors, improvement of material synthesis theory and *in situ* detection technology at the microscale, and transition from theoretical testing to commercial applications. In short, microreactors provide new ideas and methods for the synthesis of micro/nanomaterials, which have huge potential and inestimable possibilities in large-scale production and scientific research.

1. Introduction

To date, a plethora of micro/nanomaterials with easily tunable sizes, structures, and compositions have been exploited tremendously owing to their marvelous features, such as quantum tunneling effect, size effect, surface and boundary effects, and Coulomb blockade effect.[1–3] They have an increasingly significant role in various fields, including optoelectronics,[4–6] environmental materials,[7–9] bioimaging,[10–12] agricultural industries,[13–15] and drug delivery.[16–18] Therefore, micro/nanomaterial processing belongs to the manufacturing and application of materials to achieve industrial product design at the micro- or nanoscale; it is one of the most interesting industries of the 21st century and is considered to have potential as large as the IT and biotechnology fields.[19,20] Traditional preparation methods involve batch reactions in laboratory fume hoods, which can synthesize high-quality solid materials in multi-gram quantities without the need for specialized equipment.[21,22] However, the drawback of relative inflexibility in conventional batch-based synthesis methods has led to a growing interest in microfluidic wet-chemical

[a] *Faculty of Metallurgical and Energy Engineering, Kunming University of Science and Technology, Kunming, Yunnan 650093, China. E-mail: yinsh@kust.edu.cn, lswei11@163.com, zhanglibopaper@126.com*
[b] *State Key Laboratory of Complex Nonferrous Metal Resources Clean Utilization, Kunming University of Science and Technology, Kunming, Yunnan 650093, China*
[c] *Key Laboratory of Unconventional Metallurgy, Kunming University of Science and Technology, Kunming 650093, Yunnan, China*

synthesis, which has enabled the development of continuous manufacturing processes.

Microfluidics is a system technology and science that systematically manipulates or processes small (10^{-9}–10^{-18} L) amounts of liquids using integrated channels with dimensions of tens to hundreds of micrometers.[23] Microreactors are not only the miniaturization of large reaction platforms but can also be used to quickly perform multiple reactions and operations in tiny units. The microreactor represented by the microchannel provides an efficient and stable method for the production of chemical materials, and it has the advantages of controllable product properties, high recovery rate or selectivity, small reaction volume, low energy consumption, and considerable economic benefits.[24–26] The development overview of micro/nanomaterials synthesized by microreactors is shown in Fig. 1. At the beginning of nanotechnology in 1959, Late Richard Feynman, a Nobel Prize-winning physicist, made micromachining a real boom by defining micrometer-scale motors

Jianfeng Ran

Jianfeng Ran is presently a master's degree candidate under the supervision of Prof. Shaohua Yin in the Kunming University of Science and Technology, China. His research interests focus on the efficient use of rare earth resources, outfield intensifying metallurgy and advanced oxidation processes (AOPs).

Xuxu Wang

Xuxu Wang is currently a master's degree candidate under the supervision of Prof. Shaohua Yin in the Kunming University of Science and Technology, China. His research interests focus on hydrometallurgy and advanced oxidation processes (AOPs).

Yuanhong Liu

Yuanhong Liu is currently a master's degree candidate under the supervision of Prof. Shaohua Yin in the Kunming University of Science and Technology, China. Her research interests focus on the preparation of nano-rare earth oxides by microchannel coupled ultrasonic technology.

Shaohua Yin

Shaohua Yin obtained her doctorate from Northeastern University in 2013. Currently, she is working at the Kunming University of Science and Technology, China. Her primary research interests include outfield intensifying metallurgy, the solvent extraction of rare earths and the efficient use of rare earth resources.

Shiwei Li

Shiwei Li obtained his doctorate from Northeastern University in 2013. Currently, he is working at the Kunming University of Science and Technology, China. His primary research interests include outfield intensifying metallurgy, hydrometallurgy, and comprehensive recovery of the wastes in metallurgy fields.

Libo Zhang

Libo Zhang is a PhD supervisor at the Kunming University of Science and Technology, China, and mainly engages in the microwave heating and ultrasonic technology applied in metallurgy, chemical engineering, materials, etc.

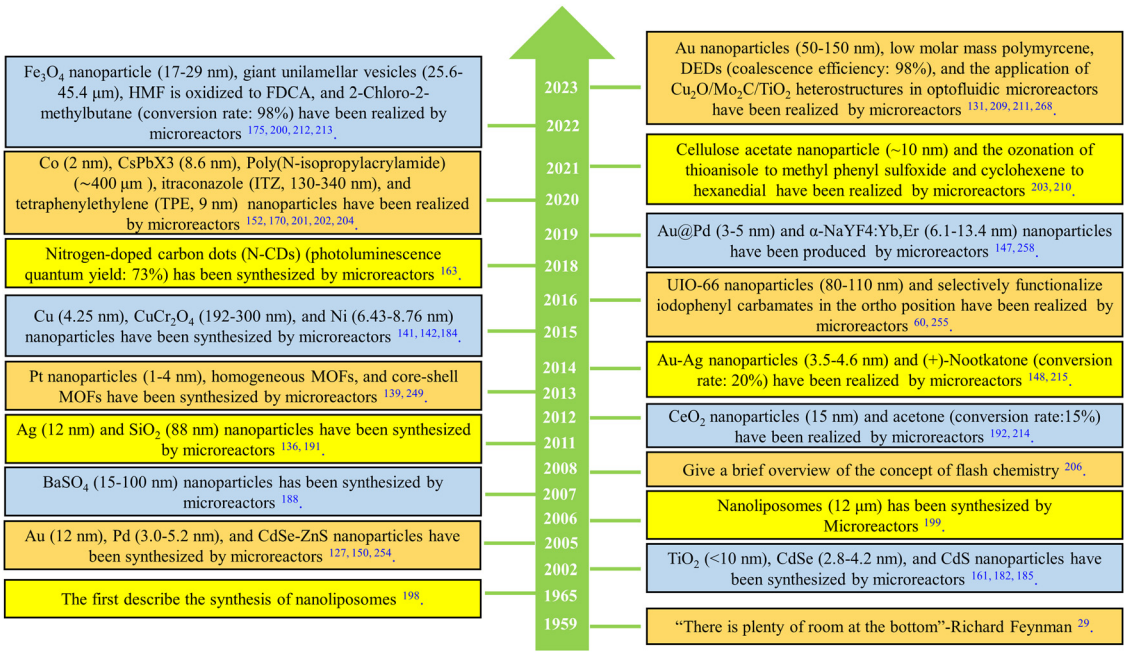

Fig. 1 The development overview of micro/nanomaterials synthesized by microreactors.

in a lecture titled, "There is plenty of room at the bottom" at the California Institute of Technology, Pasadena, CA.[27–29]

Nowadays, microreactor technology has been expanded from micromachining in a narrow sense to a subject category with a broad micro concept, including "mTAS" (micro total analysis systems), "MEMS" (micro electro mechanical systems), "Lab-On-Chip", and "BioMEMS". Systems based on micro-concept nanodevices, chips, and capillaries have emerged as promising tools in the fields of chemistry, process engineering, and biotechnology.[30] Microreactors have shown mass transfer rates and excellent heat, and the contact time, interface shape, and size between fluids can be easily and precisely controlled.[31,32] In addition, it has other benefits, such as higher conversion and selectivity,[33,34] efficient mixing,[35] reduced environmental burden and improved process safety, through the minimization of solvent and reagent quantities.[36] The basic structure of the microreactor system is a microchannel, and some additional structures need to be integrated for its functionality. One approach involves using a solid substrate on which a microchannel is positioned to form a chip and connecting fluid lines to form a microreactor unit. In general, microreactor types have been developed for different applications, including typical reactors (such as capillary reactors, plate reactors, and laminar flow reactors), parallel and series reactors, and network reactors (Fig. 2). Tubular microchannels, the simplest and most common type of microchannel, are simple, straight or curved tubes etched onto a microchip. To enhance the effect of mixing and separation, various structures can be integrated into the microchannels, such as nozzle injections,[37] micromixers,[38,39] and zigzag flow barriers.[40] By simply manipulating the inlet design of the microchannel, various flow patterns can be obtained. Y-, T- and ψ- are the most common entry design patterns. However, although these are valuable advantages,

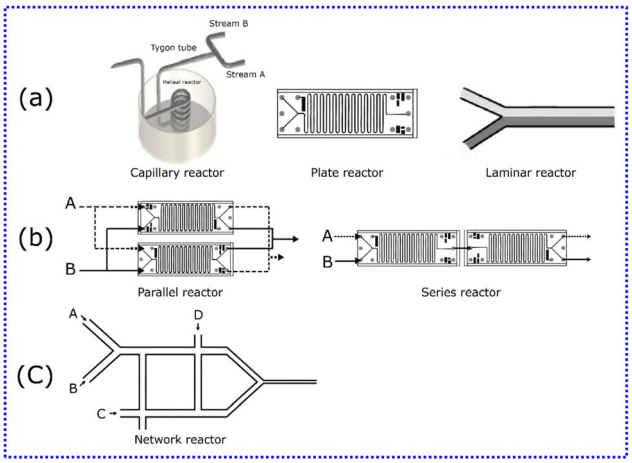

Fig. 2 Microreactor types: (a) typical reactor, (b) parallel and series reactors, and (c) network reactor.[43] Copyright 2020, MDPI.

microreactor technology has not been as widely accepted as expected. This may be because many aspects of this new technology are covered by patents.[41,42] The lack of freedom to operate is a major deterrent on the road to the industrialization of microreactors. Because several of the earlier patents have now expired, it is time to reassess the potential of microreactors and continuously operating microfactories.

This study critically provides an overview of the advancements made in the design and modification of microreactor structures and includes progress in the synthesis of micro/nanomaterials and their potential applications. Specifically, it is organized into the following sections: (1) introduction, (2) fabrication and design principles of microreactors,

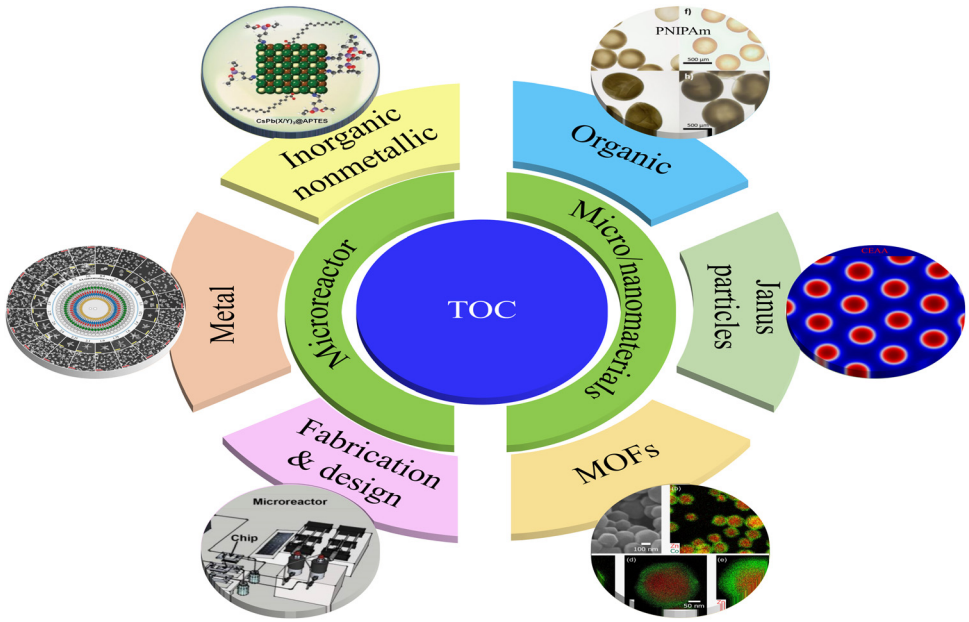

Fig. 3 Layout structure of this review. Highlighting the fabrication, design principles and applications of microreactors for the synthesis of inorganic, organic and composite micro/nanomaterials.

(3) synthesis of micro/nanomaterials by microreactors, and (4) conclusions and outlook (Fig. 3). We hope that it will provide useful help or suggestions for researchers in this field.

2. Fabrication and design principles of microreactors

The vast literature on microreactors may be a barrier for researchers familiar with conventional reactors to enter the field. To date, many famous companies and universities around the world have carried out in-depth research on microreactors, such as IMM (Institute of Microtechnique Mainz, Germany), Karlsruhe University (Germany), Merck Company (Germany), Bayer Company (Germany), Siemens Company (Germany), DuPont Company (USA), MIT (Massachusetts Institute of Technology, USA), Corning Company (France), Syrris Company (UK), Shell Company (UK), Tsinghua University (China), DICP (Dalian Institute of Chemical Physics, China), ECUST (East China University of Science and Technology), Beijing University of Chemical Technology (China), and Kunming University of Science and Technology (China). Thus, the fabrication and design principles of application-specific microreactors are first systematically discussed.

2.1. Fabrication of microreactors

The microfluidics market was estimated to be USD 1.6 billion in 2013.[44,45] With an estimated compound annual growth rate (CAGR) of 18–29%, the market is expected to grow to USD 8.4–20.4 billion by 2023.[44] This high growth rate is largely due to the development of miniaturization and the functional diversification of reactive platforms. This significant achievement may be attained through innovative and efficient design, the exploration of new materials suitable for microreactor processing, and the assembly of multiple unit operations into a single device. To date, a variety of materials suitable for microreactor processing have been developed, such as polymers, silicon, metals, stainless steel, glass, and ceramics. As shown in Fig. 4, microreaction devices can be classified into two groups: microcapillaries and chips.[46]

Microcapillary reactors are mainly used in chemical processes to achieve higher yields and conversions and are usually fabricated from appropriately sized tubular materials.[47,48] Multiple studies have shown that microcapillary reactors can enhance heat transfer and mass transfer in reactions.[49] Compared with other materials, the glass-type microcapillary reactor still maintains high resolution at a tiny scale, which makes such devices suitable for better control of the synthesis of emulsions and polymer nanoparticles. However, chip-based microreactors are fabricated using glass, silicon, or plastic through wet etching, micromachining, and soft lithography technology.[50,51] Chip-based microreactors usually comprise multiple microchannels connected by unique structures, which are used to regulate spatiotemporal changes in tiny fluids. Similar to microcapillary reactors, glass also provides chip-type microreactors with the advantage that the reaction process can be clearly observed, but owing to the difficulty in establishing structures with high aspect ratios, there are great limitations in microreactor design. Therefore, the chip-type microreactor has the advantages of easy regulation of the microfluidic flow rate and the assembly of a series of unit operations into one reactor.[52]

Specifically, the current main methods of manufacturing microreactors include numerical control micromachining,[53] laser ablation,[54] inkjet printing,[55] photolithography,[56] dry

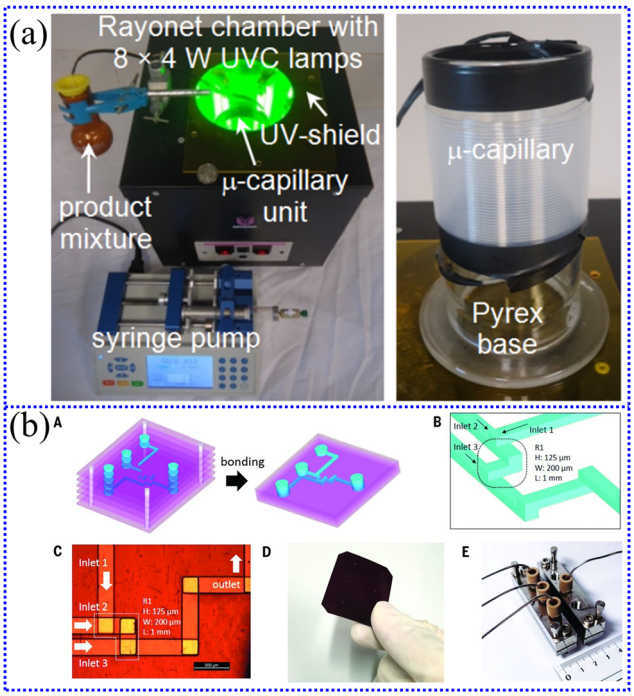

Fig. 4 (a) Microcapillary reactor: setup with inserted μ-capillary unit and μ-capillary unit.[59] Copyright 2013, Beilstein-Institut Zur Forderung der Chemischen Wissenschaften. (b) Chip microreactor (CMR) fabricated with six layers of polyimide films.[60] Copyright 2016, The American Association for the Advancement of Science.

etching,[57] and lithography, galvanoformung and abformung (LIGA) technology.[58] Some commonly used technologies for fabricating microreactors are as follows.

2.1.1. Lithography, galvanoformung and abformung (LIGA) technology. LIGA technology, first reported at Karlsruhe nuclear research center in Karlsruhe, Germany, in 1990, is an important microreactors fabrication process.[61–63] LIGA refers to lithography, electroplating, and molding, which corresponds to the acronyms of lithographie, galvanoformung and abformung in Germany. The application of this technology has proven useful based on which microreactors can be easily processed through various materials, including metallic species, polymer substances, and plastic materials. As the name lithography implies, this process is employed in combination with other groups of light sources, including X-ray radiation and UV light. X-ray radiation is used for features with a high aspect ratio, whereas UV light is used for structures with a relatively low aspect ratio.[36,64,65] Moreover, to optimize the cost of X-ray-based lithography, cheaper lithography light sources and mask manufacturing processes have emerged. For example, laser-LIGA technology uses an excimer laser as a light source for lithography,[66] and mask making by micro electro-discharge machining (EDM) technology.[67]

Generally, the LIGA technique comprises three phases: (i) the pattern is transferred to a photoresist (which is typically a resin-type material placed on an electrically conductive or conductive coating), (ii) removing the mask and any undesirable structural layers and electroplating by the short wavelength X-ray radiations to form a relief structure onto the substrate area, and (iii) the withdrawal of the excess electrodeposited material and photoresist or epoxy after metal structures are formed by photoirradiation.[68–70] The specific steps of LIGA are shown in Fig. 5.

Microreactors processed by LIGA technology can also be used in biomedical fields, such as extracting deoxyribonucleic acid (DNA). Effenhauser *et al.*[71] from Novartis Pharma AG in Switzerland fabricated a polydimethylsiloxane (PDMS)-silicon-based microreactor for isolating DNA and creating micro-channels from the silicon semiconducting substance, followed by cleaning off the solidified plate. PDMS technology is used to form an integrated device, and specific processes include photolithography, electroplating, and molding. However, some limitations of LIGA technology must be considered, including the radiation threat to the operator using high-energy X-rays, the difficulty of managing the multi-step process, and the high cost of special equipment.

2.1.2. Micromachining technology. The broad concept of micromachining technology includes various technical routes,

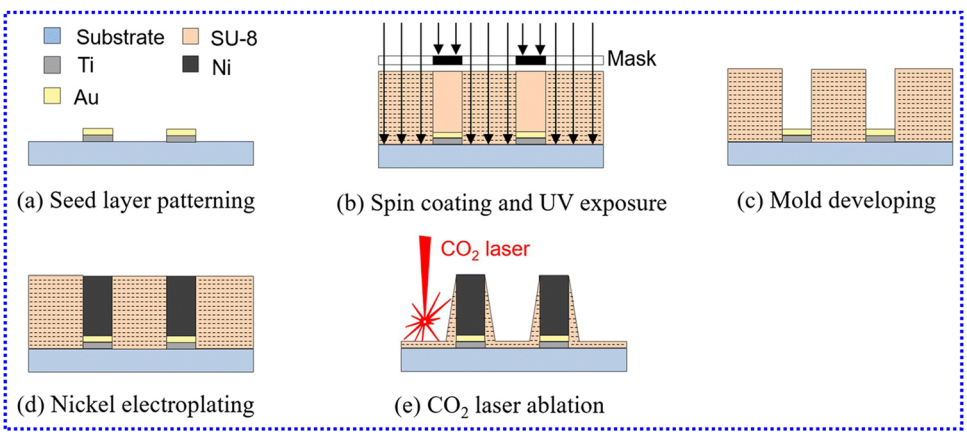

Fig. 5 The specific steps of LIGA. (a) Seed layer patterning. (b) Spin coating and UV exposure. (c) Mold developing. (d) Nickel electroplating. (e) CO_2 laser ablation.[72] Copyright 2020, Springer Nature.

and there are many operating units in the industrial field. The miniaturization trend of products and their components has become increasingly obvious in the industrial field, especially in the construction and application of MEMS, including photolithography, chemical etching, electroplating and LIGA technology. The practice has found that various microreactors can be processed by MEMS technology and are then widely used in the field of chemical analysis or the manufacture of special chemicals.[73,74] They are also widely used in the mass production of semiconductors or microelectronics, mainly including sensors and actuators machined from silicon or parts of metal. However, as a new category of microfabrication technologies, non-MEMS or non-lithography-based micro manufacturing has been rapidly developed in the last two decades. Micro extrusion, micro mechanical cutting, micro EDM, micro stamping, micro laser cutting/patting/drilling, micro embossing, and micro injection moulding are involved in the non-lithography-based micro manufacturing field. The classification of micromachining technology is shown in Fig. 6.

Two key technical challenges, such as creating microfeatures and generating micro-/nano-level finished surfaces, can be employed through micromachining processes. Moreover, micromachining is a useful technology for creating specific surface topography, forms that require several sides and specific geometries, and physically drilling holes in a substance using an electron beam instrument.[75,76] Compared with other technologies, this technology is used at a lower cost for microreactor production. Specifically, micromilling is readily available and relatively inexpensive for three-dimensional (3D) metal fabrication of brass, aluminum, and stainless steel materials. However, the disadvantages of relatively high roughness, poor surface quality, and a low aspect ratio of microfeatures are worthy of focus. Mechanical precision machining with tools made of diamond or cubic boron nitride (CBN) is one of the most suitable techniques for achieving the best surface quality.[77] However, the overall cost, including tooling and time required for mechanical precision machining, can be high. EDM is a promising microreactor manufacturing process that emerged at the end of the 20th century.[78,79] The discharge of the loaded electrode between the workpiece and the tool allows excess material on the workpiece to be removed by the electrical heating process.[80] The mechanism of EDM is shown in Fig. 7, which includes the following stages. In the first stage, a gap voltage is applied between the electrode and the workpiece, causing an electric field to appear between them. In the second stage, the servo controller regulates the gap between the electrode and the workpiece. The proper distance makes the electric field more concentrated than the dielectric strength. Subsequently, the enhanced electric field causes the dielectric to break down, and an electric spark is generated. In the third stage, the appearance of the electric spark causes the plasma channel to be expanded, pushing the ionized particles to move towards the anode and cathode, and this process converts kinetic energy into heat. Consequently, high temperatures ranging from 8000 °C to 12 000 °C are generated in the plasma column.[81–83] Under this condition, affected by the melting and vaporization produced by the high temperature, the material begins to fall off from the workpiece, and the dielectric fluid is also evaporated, producing gases and fumes. In the final stage, the plasma column disappears, and the eroded material is redeposited as defects or debris in the processing cavity, eventually forming the crater. Compared with ultra-precision micromilling, EDM can achieve better surface flatness by controlling the machining quality and tool path. However, it also has drawbacks, such as inaccessible machines and a slow machining process.

2.1.3. Etching technology. Etching technology includes two main forms: wet etching (using acid) and dry etching (using gas), belonging to the field of photochemical technology and is widely used in processing thin precision metal products.[85,86]

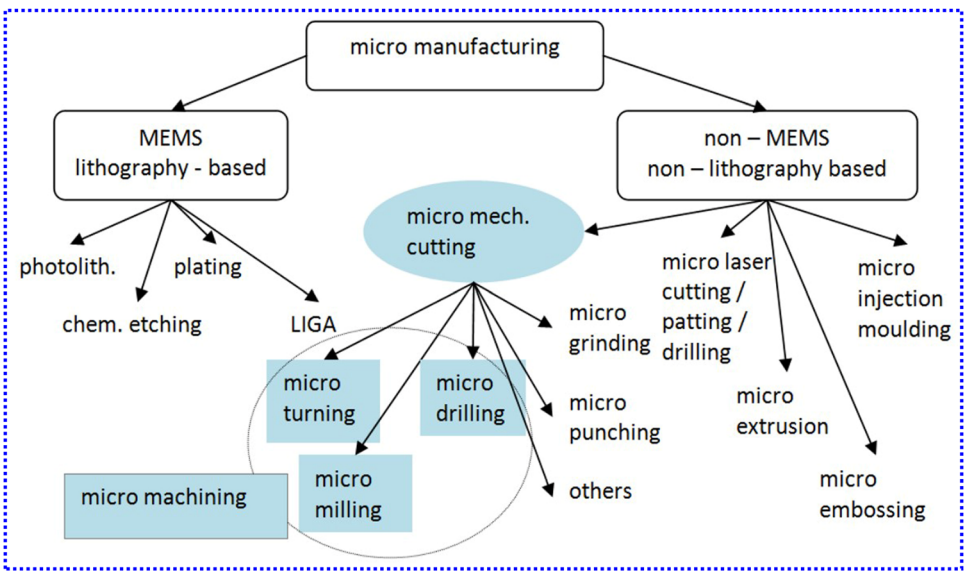

Fig. 6 Classification of micromachining technology.[84] Copyright 2014, Croatian Interdisciplinary Society.

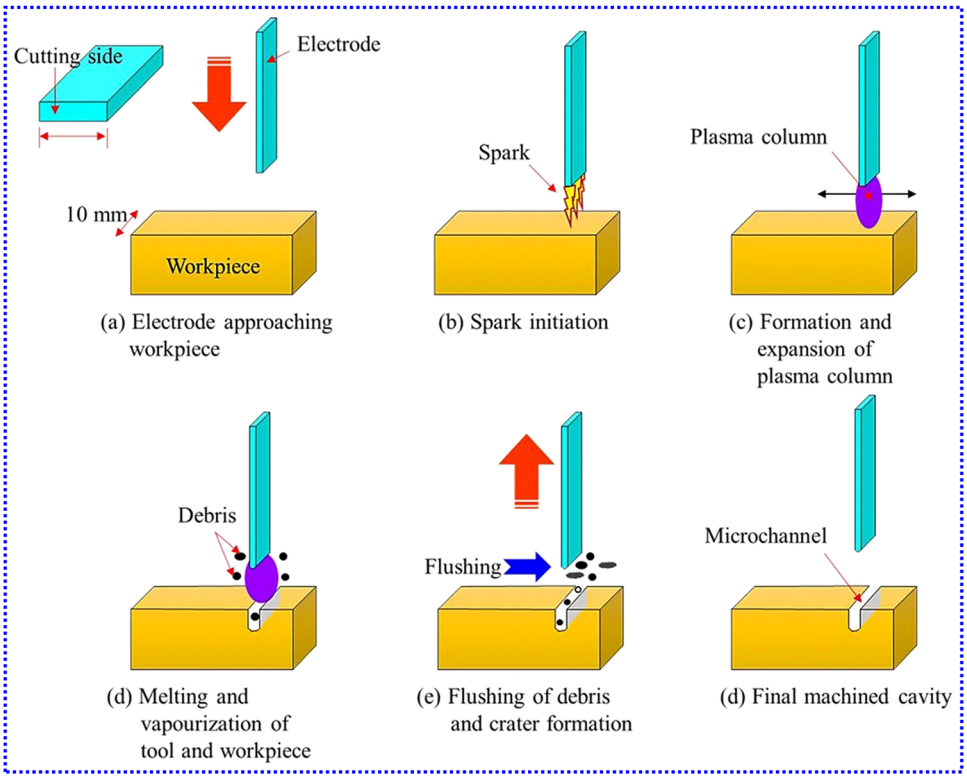

Fig. 7 Working mechanism of the EDM process for the fabrication of microchannel.[81] Copyright 2022, Springer Nature.

Wet etching can be easily implemented on a routine laboratory scale and is commonly used in glass processing and the production of microchannels in laminar flow systems, whereas industrial mass production usually requires dry etching, which may require a large one-time investment and high maintenance costs.[87] In general, when the material is wet etched, the processing rate in the vertical and horizontal directions is the same, while in dry etching, the plasma can be used for anisotropic processing at a specific position in the etching chamber. In addition, photosensors are often used in the etching process of metallic materials. This etching process involves applying a photosensitive layer mask to the metal to be processed, where the presence of the molecular layer helps orient the photosensor to the light source. The primary mask containing the structural layer is used for exposure, and the exposed part is then polymerized. To date, various exposure methods and photosensitive mask materials have been explored. Then, the unexposed part is directly dissolved in a chemical solution.[88]

The optimal ratio of abundant species in the wet etching process has been confirmed to be in the range of 0.5–0.6, while the standard ratio of the dry etching process has not been determined, as it is one of the most expensive techniques available. Wet etching is the formation of a half-circular structure that is visible owing to the use of an isotopic abundance system. An excellent example of a wet etching process is illustrated in the Pyrex glass, as shown in Fig. 8(a). In contrast, various geometric structures with varying aspect ratios can be formed by the dry etching process. Kothare[89] from Lehigh University in the USA demonstrated that the construction of microchannels has a depth range of 200–400 μm and a width of 1000 μm, while Suryawanshi *et al.*[90] from the National Institute of Technology in India also illustrated the fabrication of various microchannel sizes and forms to synthesize nanoparticles $\geq$5 nm at a flow rate of 14 μL s^{-1}, as shown in Fig. 8(b) and (c). The core is still in contact with the reactant through the substrate in these processes, so the wet etching process is principally identical and independent of crystalline orientation.

Furthermore, selectivity is a vital influencing factor during these processes, which means that there is a strong relationship between the printing rate and the raw material to be processed. Selectivity varies mainly between the photosensor and the raw material in wet etching, so the material can be etched at different rates in certain directions, resulting in two main forms: anisotropic and isotropic etching. The former means that the plasma etches vertically in one direction, whereas the latter means that the plasma etches in all directions.[92,93] Both of the above printing and etching methods have been implemented in Thierry's low-pressure plasma system.[94–96] For wet etching, such as etching silicon on semiconductor material substances, an etchant is preferred. Anisotropic wet etching is an important process for fabricating nanostructures that are widely used in silicon-based devices.[97,98] Tetramethyl ammonium hydroxide (TMAH) and potassium hydroxide (KOH) solutions are considered the most commonly used anisotropic etchants in the semiconductor industry. Hydrofluoric (HF) acid/nitric acid (HNO_3)

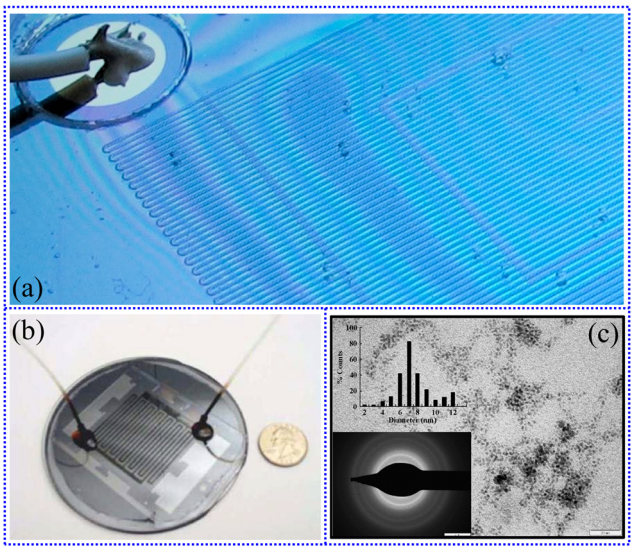

Fig. 8 (a) Enlarged view of the microreactor showing the network of microchannels etched in Pyrex glass.[91] Copyright 2020, MDPI. (b) View of the final microreactor device.[89] Copyright 2006, Elsevier. (c) Nanoparticle size and crystallinity observed by TEM and SAED in a continuous flow microreactor.[90] Copyright 2016, Elsevier.

mixtures are the most common isotropic etchant for silicon wafers and have been widely used to eliminate saw-damage and create MEMS structures, including deep holes and channels.[99,100] In summary, the advantages and disadvantages of various fabrication technologies for microreactors are compared, as shown in Table 1.

2.2. Design principles of microreactors

Such microreactors for chemical synthesis are often difficult to accept owing to some conceptualization principles, implying a different schematic basis for microreactor scale-up, which is usually laminar continuous flow. The batch information of process designs makes it easy to minimize problems and meet industrial requirements. Additionally, complex chemical reactions can be carried out using microreactors; therefore, they are preferable for industrial large-scale production of synthetic materials or chemicals. This is due to the ability of microreactors to operate on the concept of small surface areas, which means that the frequency of molecular collisions is kinetically and significantly increased, ultimately speeding up the production of products. Broadly, these complex chemical reactions carried out in microreactors usually involve multiple phase states that do not mix, which can be divided into liquid–liquid reactions[27,101,102] and gas–liquid reactions.[103–105] However, the mixing process in microchannels of small volume is not governed by the same laws as macroscale mixing but instead mainly occurs in chaotic advection and involves a laminar regime. The functional design of the microreactor elements used can greatly influence mixing efficiency.

Based on the existence of interexternal bonding powers and mechanical agitation, the mixing that occurs in microreactors can be categorized into two types: passive and active mixing.[106–108] Active mixing operates often involve kinetic energy-based disturbance energies, such as electrokinetic, acoustic waves, electrowetting, magnetic, and electromagnetic, so special requirements are placed on the structural design of microchannels.[109–111] Acoustic streaming produced by cavitation is effective for mixing with ultrasonic applications because it causes flow agitation. In particular, sonolysis causes microbubbles in the liquid to rupture owing to cavitation and creates microjets and flows, which enhance mixing. With the cooperation of Universiti Malaysia Sarawak (UNIMAS, Malaysia) and Shibaura Institute of Technology (Japan), Mahmud *et al.*[112] reported the effect of ultrasonic and thermal energies on the mixing of microfluidics and showed that both factors are potentially useful in mixing; at Reynolds numbers (Re) between 5 and 100, the mixing efficiency of the ultrasonic mixer increases from 6% to 10% as the temperature increases from 30 °C to 60 °C, and the qualitative images of the experimental results are shown in Fig. 9(a), respectively. Additionally, the application of a magnetic field achieves the purpose of rapid mixing, which mainly acts on magnetic beads by stirring the fluid with the magnetic field. Shyam *et al.*[113] from the Indian Institute of Technology in India reported the mixing of ferromagnetic droplets with nonmagnetic miscible fluids in the presence of a time-varying magnetic field, and they showed that magnetic nanoparticles exhibit complex spatiotemporal motions within the ferrofluid droplet domain in a transient magnetic forcing environment, thus improving mixing efficiency in the convective mixing region. Under the influence of various magnetic field frequencies, the variation vorticity contours in the ferrofluid droplet flow field

Table 1 Comparison of various fabrication technologies for microreactors

Category	Advantages	Disadvantages
LIGA	Higher processing precision Higher processing efficiency Wider range of applications	Higher radiation threat from high-energy X-rays More difficulty in managing multi-step processes Higher cost of special equipment
MEMS (lithography-based)	Lower processing cost	Poor surface quality Lower aspect ratio
Non-MEMS (non-lithography-based)	Better surface flatness	Inaccessible to machines Slower processing
Wet etching	More suitable for routine laboratory scale Faster processing speed	More difficult to control the shape More serious environmental pollution
Dry etching	More suitable for industrial mass production Higher processing precision Easier to realize automation	Larger one-time investment Higher maintenance costs

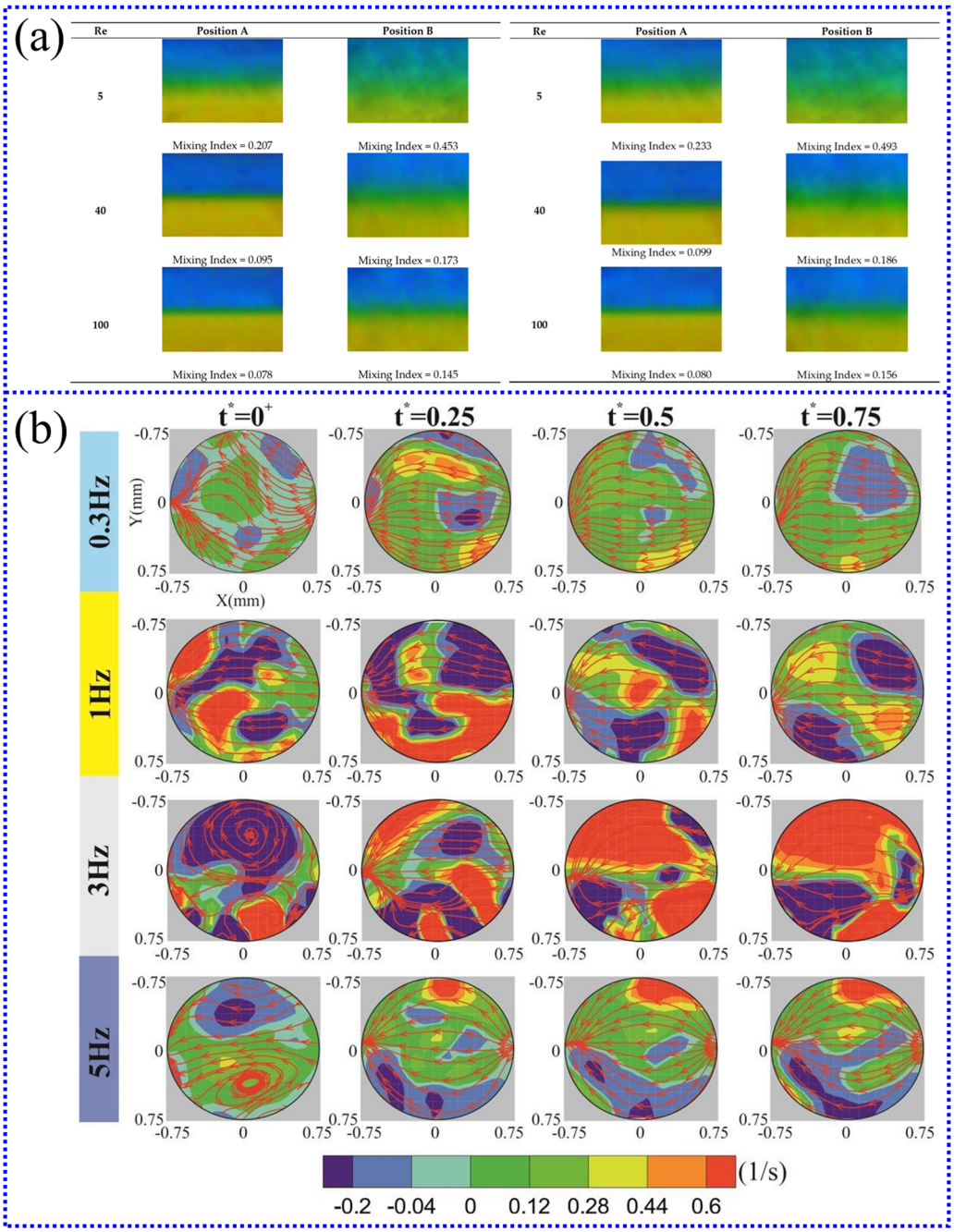

Fig. 9 (a) Captured mixing images and mixing index of micromixer using 40 kHz ultrasound at 30 °C (left) and 60 °C (right) for Re = 5, 40 and 100 (image size: 250 × 174 μm^2).[112] Copyright 2021, MDPI. (b) Plot depicting the temporal variation in the vorticity contours for the various magnetic field frequencies of 0.3 Hz, 1 Hz, 3 Hz, and 5 Hz. The red arrows indicate the streamlines of the flow. The plot shows the vorticity flow field when the right magnet is in ON state.[113] Copyright 2021, Cambridge University Press.

are shown in Fig. 9(b). It is found that the vorticity is maximum at 3 Hz, which agrees with the experimental phenomenon.

However, based on the mechanism of diffusion, passive technologies increase the contact area by stretching or layering the fluid.[114–116] Passive mixing is a better process for multi-layer micro-mixing systems in the industry, which can significantly improve the yield of chemical synthesis. Passive methods generate secondary flow by designing complex channel geometries to improve the efficiency of multiphase micromixing, which mainly includes pattern design in the channel, obstacle filling in the channel, and various channel geometries, such as serpentine. Through the passive enhanced fluid mixing of chaotic advection, Liu *et al.*[117] from the University of Illinois in the USA proposed a design of a three-dimensional serpentine microchannel, as shown in Fig. 10(a). They found that when Re is 70, the phenolphthalein produced by the serpentine channel

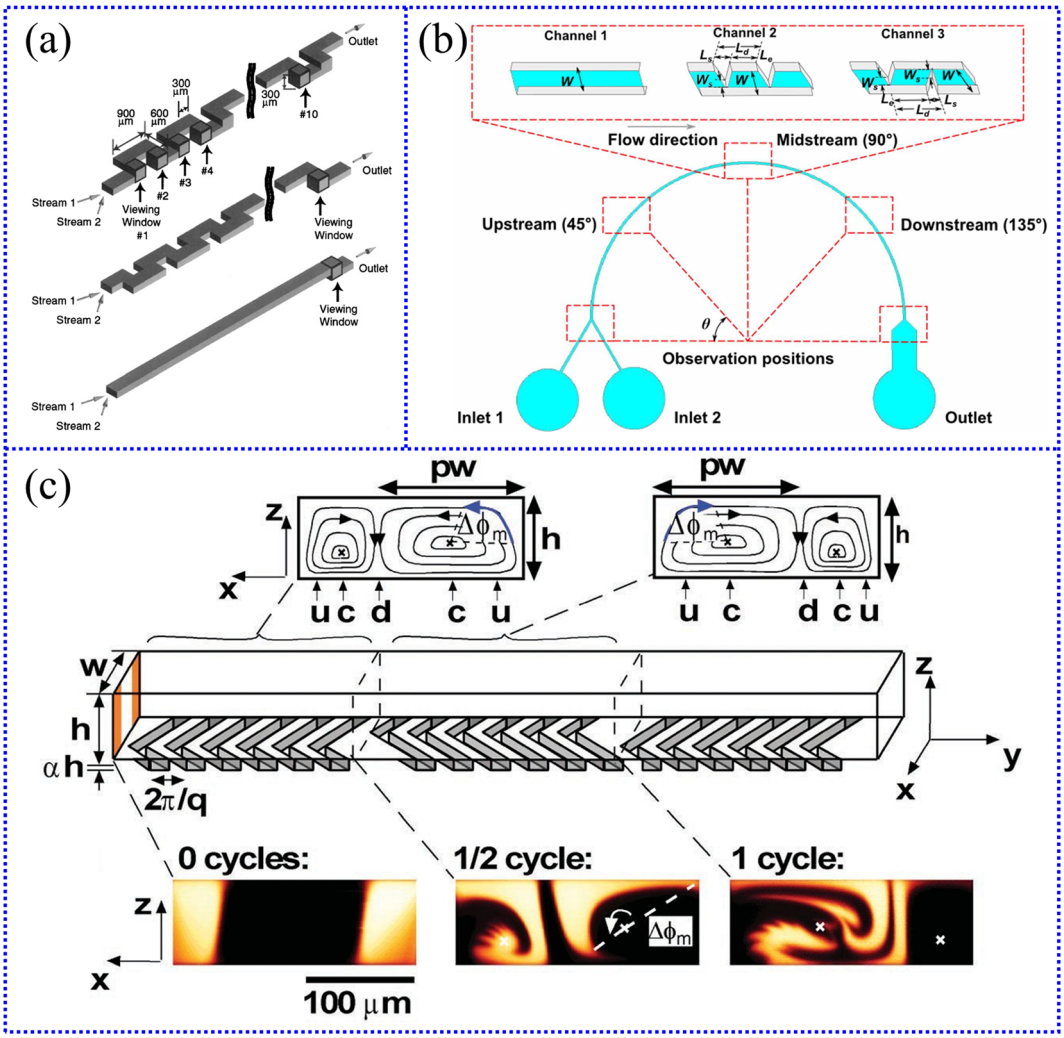

Fig. 10 (a) (Top) Schematic of the three-dimensional serpentine channel, "viewing windows" in the channel are labeled 1–10; (middle) schematic of square-wave channel; and (bottom) schematic of straight channel.[117] Copyright 2000, IEEE. (b) Schematic diagrams of arc microchannels, including simple arc microchannels (channel 1), arc microchannels with sharp corners located on external walls (channel 2) and asymmetrically located on both side walls (channel 3).[118] Copyright 2021 IOP, Publishing Ltd. (c) Staggered herringbone mixer (SHM).[119] Copyright 2002, The American Association for the Advancement of Science.

is 16 times that of the straight channel and 1.6 times that of the square-wave channel. The mixing rate in the serpentine channel at high Re agrees with the occurrence of chaotic advection. Visualization of the interface formed in the channel between the water stream and the ethanol revealed that mixing is a combination of diffusion and fluid agitation. With the cooperation of Xi'an Jiaotong University (China) and the University of Akron (USA), Huang *et al.*[118] proposed a novel microfluidic device for efficient passive mixing, that is, a series of sharp corner structures designed on the side wall of an arc microchannel, as shown in Fig. 10(b). They demonstrated that compared with the simple arc microchannel, the three-dimensional vortices are created in the arc microchannels with sharp corners. Further, chaotic advection and molecule diffusion are significantly enhanced. Consequently, the mixing efficiency of the fluid can reach from ~87% to 92% when the Re is in the range of 3.0–24.2. In addition, the effect of obstacle position on mixing within the curved channel is investigated, and it is shown that obstacles on the outer side walls can induce better mixing than obstacles located asymmetrically on both sides. Stroock *et al.*[119] from Harvard University in the USA illustrated a design scheme of interlaced herringbone patterns embedded in microchannels, as shown in Fig. 10(c). They observed that the mixing efficiency could reach about 90% at a higher Peclet number and a channel distance of 1.7 cm, suggesting that the staggered herringbone design can be used to generate chaotic flow in environments other than pressure-driven flow in microchannels. Specifically, the geometric asymmetry of the structure leads to the rotation and extension of the local flow and the switching of the flow centerline, resulting in chaotic flow and significantly improved mixing efficiency.

Nowadays, analytical simulations of operating processes in microreactors are usually performed using various computer software.[120–122] For a given chemical reaction, the microchannel

size and flow rate of some specific microreactors can be simulated by computer technology to solve complex multiphysics problems on the length scale of microreactors. Such software, including CoventorWare, computational fluid dynamics (CFD)-ACE+, Fluent, and COMSOL Multiphysics, is used to study liquid-fluid behavior in microreactors under various geometries, solve numerical equations describing microreactor systems, and optimize by combining all model systems. These computer software programs make the design of small reactors simpler and more accurate, so they significantly reduce labor costs in the industry, thus promoting the large-scale application of microreactors. However, microreactors, which are usually operated as continuous flow systems, in which the dynamic balance of heat and mass transfer must be considered. Currently, the production of microreactors has become much simpler. If parameters regarding heat transfer, mass transfer, momentum transfer, and kinetic equations are properly entered into the software, the output of microreactor details and chemical reaction conditions becomes very detailed. In addition, boundary methods, including finite element, volume, and part strategies, are used to specify initial and boundary conditions, which are subsequently translated into computer-based codes. This operation helps refine the fundamentals of microreactors, including mathematical prototypes, and linear kinetics, including continuous laminar flow. Then, a means needs to be provided to parse the desired microreactor-related simulation results. Finally, the optimal design process of the microreactor is proposed, and the corresponding processing is carried out. Early in the 21st century, Ferziger *et al.*[123] from Stanford University in the USA described these methods in great detail and discussed many examples such that their work has been called a guide to numerical methods for solving fluid dynamics problems. In this book, they describe in detail the most widely used discretization and solution methods, which are also found in most commercial CFD programs. Some advanced topics, such as moving meshes, turbulent flow simulations, calculations of free surface flows, multigrid methods and parallel computing, are also covered. In short, it is definitely a great pioneering work in this field that computers are widely used in the analysis of the operation process of microreactors, greatly speeding up the design and large-scale application of microreactors.

3. Synthesis of micro/nanomaterials by microreactors

Compared with their macroscopic materials, micro/nanomaterials owing to the size difference exhibit various physical, chemical, optical, and mechanical properties and have great application potential in many aspects. The micro/nanomaterial synthesis system based on microreactors can provide an integrated platform that integrates design, synthesis and detection. From the perspective of physical and chemical properties, micro/nanomaterials can be divided into three categories: inorganic, organic and composite materials. Thus far, microreactors have been widely used in the synthesis of these three types of micro/nanomaterials.

3.1. Synthesis of inorganic micro/nanomaterials

3.1.1. Metal micro/nanomaterials. Metal micro/nanomaterials, such as gold (Au), silver (Ag), copper (Cu), platinum (Pt), and palladium (Pd), have attracted considerable attention in the past few decades due to their size- and shape-dependent properties and have a substantial impact on a broad range of applications, such as electronics, optics, catalysis, biomedicine, and sensors.[124–126] However, they are difficult to prepare into the desired particle size distribution using traditional methods because they often suffer from agglomeration and precipitation owing to the principle of energy minimum. However, the physical and chemical properties of synthesized micro/nanomaterials significantly depend on their special structures. Therefore, heat and mass control play an important role in the formation of metallic micro/nanomaterials. In summary, microreactors can provide important assistance for the synthesis of micro/nanomaterials because of their tiny size structures with fast heat and mass transfer characteristics.

The synthesis and modification of Au micro/nanomaterials have been researched by multiple institutes around the world. Wanger *et al.*[127–129] from the Technical University of Ilmenau in Germany provided various methods for synthesizing Au nanoparticles. First, they successfully prepared Au nanoparticles with diameters ranging from 15 to 24 nm in a chip-based interdiffusion microreactor using ascorbic acid as the reducing agent, 12 nm seeds as the nucleation center, and polyvinyl pyrrolidone (PVP) as a particle stabilizer, as shown in Fig. 11(a). The size of the produced Au nanoparticles is affected by various factors during this process, such as the flow rate and concentration ratio of reactants and the order of reactant addition. The diameter of the nanoparticles increases as the flow rate decreases, and it is possible to grow only when the seed concentration does not exceed the concentration of Au^{3+}. Second, they also directly synthesized Au nanoparticles (5–50 nm) from a gold salt ($HAuCl_4$) and reducing agent (ascorbic acid) in a glass–silicon microreactor under continuous flow conditions, as shown in Fig. 11(b). When c(PVP) = 0.25%, pH = 9.5, c($HAuCl_4$) = 1 mM, c(ascorbic acid) = 20 mM, and a total flow rate of 2000 μL min^{-1}, the average diameter of the Au nanoparticles is 5.6 nm. They provided two methods for suppressing reactor fouling: silanization of the reactor and working at an elevated pH. Silanization of the reactor results in a hydrophobic surface, making the surface less wettable and thus inhibiting reactor fouling. Moreover, working at an elevated pH, the net negative charges on the particles and the inner surfaces of the reactor repel each other, resulting in less deposition. Third, they also presented a new method for the production of Au nanoparticles in a microfluidic system. Through the direct reduction of chloroauric acid and borohydride, Au nanoparticles with a mean diameter of about 4 nm are obtained at flow rates between 200 μL min^{-1} and 4 mL min^{-1} at room temperature without obvious fouling of the reactor. The average size of Au nanoparticles hardly changes in a comparable high flow rate range, indicating that the nucleation conditions of particles in this study are independent of the flow rate. However, the increased dilution of tetrachloroaurate and borohydride makes

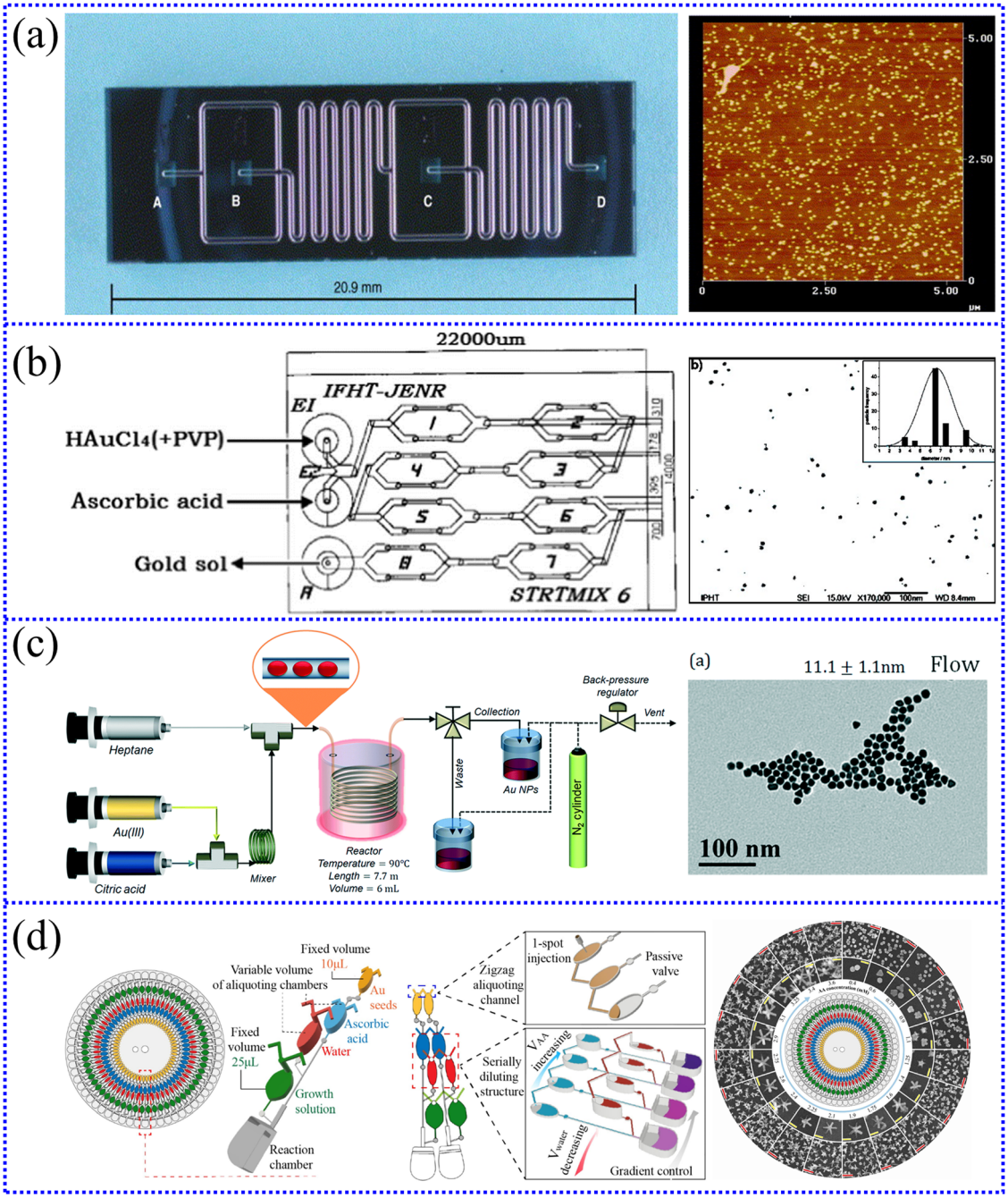

Fig. 11 (a) Photograph of the microchannel reactor and AFM image of 12 nm Au seeds.[127] Copyright 2004, Elsevier. (b) Schematic drawing of the connectivity of the IPHT microreactor and SEM image of 5–50 nm Au nanoparticles.[128] Copyright 2005, American Chemical Society. (c) Schematic of the experimental set-up used for the passivated Turkevich flow synthesis and TEM micrographs of ~11 nm Au nanoparticles.[130] Copyright 2020, Royal Society of Chemistry. (d) High-throughput centrifugal microdevice and the morphology change of 50–150 nm Au nanoparticles.[131] Copyright 2023, Elsevier.

the average diameter of the particles smaller. The growth rate is slower at lower concentrations, which means that it is harder to reach the nucleation threshold, increasing the nucleation number. Therefore, a generalized reaction equation for nucleation is proposed as follows:

$$a[M_n]^+ + R \rightarrow [M_aL_m]^{a-1} + R^+ + (na - m)L, \quad (1)$$

where M, R and L represent metal, reducing agent, and ligand, respectively; a, m, and n represent stoichiometric coefficients.

Recently, Panariello *et al.*[130] from University College London in the UK developed a flow microreactor to synthesize highly reproducible Au nanoparticles through well-established Turkevich synthesis, as shown in Fig. 11(c). The Au precursor is passivated for ~24 h to become p_Au(III) before adding

NaOH for the passivated Turkevich batch synthesis. It is found that when the synthesis temperature is 90 °C, [p_Au(III)] = 0.2 mM, [citric acid]/[p_Au(III)] = 12, ~11 nm monodisperse, Au nanoparticle can be synthesized, and its RSD (the ratio between the standard deviation and the average size) is about 10%. The pH adjustment is necessary because the ligand and the metal can be exchanged in the alkaline system, redistributing $AuCl_4^-$ into different hydroxylated forms, as shown in eqn (2)–(5):

$$AuCl_4^- + OH^- \rightleftharpoons AuCl_3(OH)^- + Cl^- \quad (2)$$

$$AuCl_3^- + OH^- \rightleftharpoons AuCl_2(OH)_2^- + Cl^- \quad (3)$$

$$AuCl_2(OH)_2^- + OH^- \rightleftharpoons AuCl(OH)_3^- + Cl^- \quad (4)$$

$$AuCl(OH)_3^- + OH^- \rightleftharpoons Au(OH)_4^- + Cl^- \quad (5)$$

Nguyen *et al.*[131] from Kyung Hee University in Korea designed a novel automated synthesis platform that is capable of 60 different reactions and can generate Au nanoparticles with diameters between 50 and 150 nm, as depicted in Fig. 11(d). Through this platform, different shapes of Au nanoparticles, such as spherical, triangular, quadrilateral, polyhedral, and star, can be prepared with different concentrations of ascorbic acid. This is because the high concentration of ascorbic acid can accelerate the reduction process and prevent the surfactant from adhering to the {111} Au facets, resulting in disordered multi-spiked particles. Additionally, excess ascorbic acid can suppress the number of positive charges on the growing seeds and accelerate the transfer of Au atoms from facets {110} to facets {111}. Their study highlights the feasibility of synthesizing high-performance micro/nanomaterials *via* centrifugal microfluidic devices and their great applicability in the discovery of new nanomaterials, drug screening, and biodiagnostics.

Zhang *et al.*[132] from Yunnan University in China introduced a new method for the synthesis of monodisperse Au nanoparticles with diameters below 10 nm, mainly through a simple and efficient microreactor based on a microfluidic chip and a liquid peristaltic pump. It is found that the best experimental results can be obtained when the temperature is 100 °C, the flow ratio is 5 : 3, and the total flow is 0.2 mL min^{-1}.

Additionally, Ag nanoparticles are mainly used in photographic reactions, catalysis and chemical analysis.[133–135] Nightingale *et al.*[136] from Imperial College London in the UK proposed a general-purpose capillary-based droplet reactor with a main capillary diameter of 0.82 mm and a distance of 20 cm from the droplet formation point to the capillary outlet. Using this microreactor, silver nitrate ($AgNO_3$) is reduced with sodium borohydride ($NaBH_4$) at room temperature, and Ag nanoparticles with an average particle size of 12 ± 4 nm are synthesized. They also successfully synthesized titanium oxide (TiO_2) and cadmium selenide (CdSe) nanoparticles using the reactor, and both operated stably and without fouling for several hours. Lintag *et al.*[137] from the University of the Philippines in the Philippines prepared Ag nanoparticles with an average size of 24 nm using PDMS microreactors with 0.001 M $AgNO_3$ and 0.002 M $NaBH_4$ as raw materials. The particle size distribution at the microscale is narrower than that at the macroscale, indicating that the Ag nanoparticles formed in the microreactor are more uniform and monodisperse. The technology is 50-fold lower than the existing commercial technology from the production cost analysis.

With the cooperation of the AGH University of Science and Technology (Poland) and the University of Adelaide (Australia), Wojnicki *et al.*[138] successfully synthesized 4H and 2H Ag nanoparticles with hexagonal structures and an average particle size of 4.4 ± 1.3 nm through a continuous-flow two-phase microdroplet system using a chemical approach and a diffusion rate-limiting step for the first time, as shown in Fig. 12(a). Peclet number (Pe) is about 2.8×10^3 in the microflow reactor compared to the batch reactor, confirming the contribution of convection to mass transfer.

Baumgard *et al.*[139] from Universität Rostock in Germany successfully synthesized Pt nanoparticles with an average diameter of 1–4 nm in three special microreactors using H_2PtCl_6 as a metal precursor and ethylene glycol as a solvent and reducing agent, as shown in Fig. 12(b). Further, it is found that the particle size of Pt nanoparticles formed inside the microstructure can be controlled by the ratio of NaOH/Pt. The Pt nanoparticles are dominated by the nucleation process at a high NaOH/Pt-ratio, and their average particle size is found to be smaller than 1.7 nm. However, they are dominated by the growth process at a low NaOH/Pt-ratio, and their average particle size is enlarged to around 3.6 nm.

Additionally, to promote the application of microreactors in the synthesis of metal nanoparticles, members of our team, such as Xu *et al.*,[140–142] conducted several studies. First, they prepared Cu nanoparticles with an average diameter of 14.15 nm at room temperature using $NaBH_4$ to reduce the copper sulfate ($CuSO_4$) solution, as shown in eqn (6). The T-shaped microreactor used is made of LIGA-treated PDMS with a length, width, and height of 10 mm, 200 mm, and 30 mm, respectively. Second, they also produced Cu nanocolloids with an average diameter of 4.25 nm at room temperature (25 ± 2 °C), putting $CuSO_4$ solution and $NaBH_4$ solution into a T-shaped microreactor (stainless steel, IMM, Germany) with a diameter of 1/16 inch. Third, they also synthesized Ni nanoparticles with a face-centered cubic (FCC) structure at 80 °C in a T-shaped continuous flow microreactor using nickel sulfate ($NiSO_4$) and hydrazine (N_2H_4) as raw materials, as shown in Fig. 12(c). The microchannel is composed of a 1/16 inch (1.58 mm) tee joint (stainless steel) that allows two liquids to react at a high-velocity flow at a millimeter-scale interface. When the flow rate increases from 15 mL min^{-1} to 35 mL min^{-1}, the average particle size of Ni nanoparticles decreases from 8.76 nm to 6.43 nm.

$$4Cu^{2+} + BH_4^- + 8OH^- = 4Cu + B(OH)_4^- + 4H_2O \quad (6)$$

Nowadays, bimetallic nanoparticles, excellent candidates for applications in catalysis, plasmonics, nanomedicine, *etc.*, owe their excellent performance to properties that depend on the overall nanoparticle structure (*i.e.*, the relative distribution

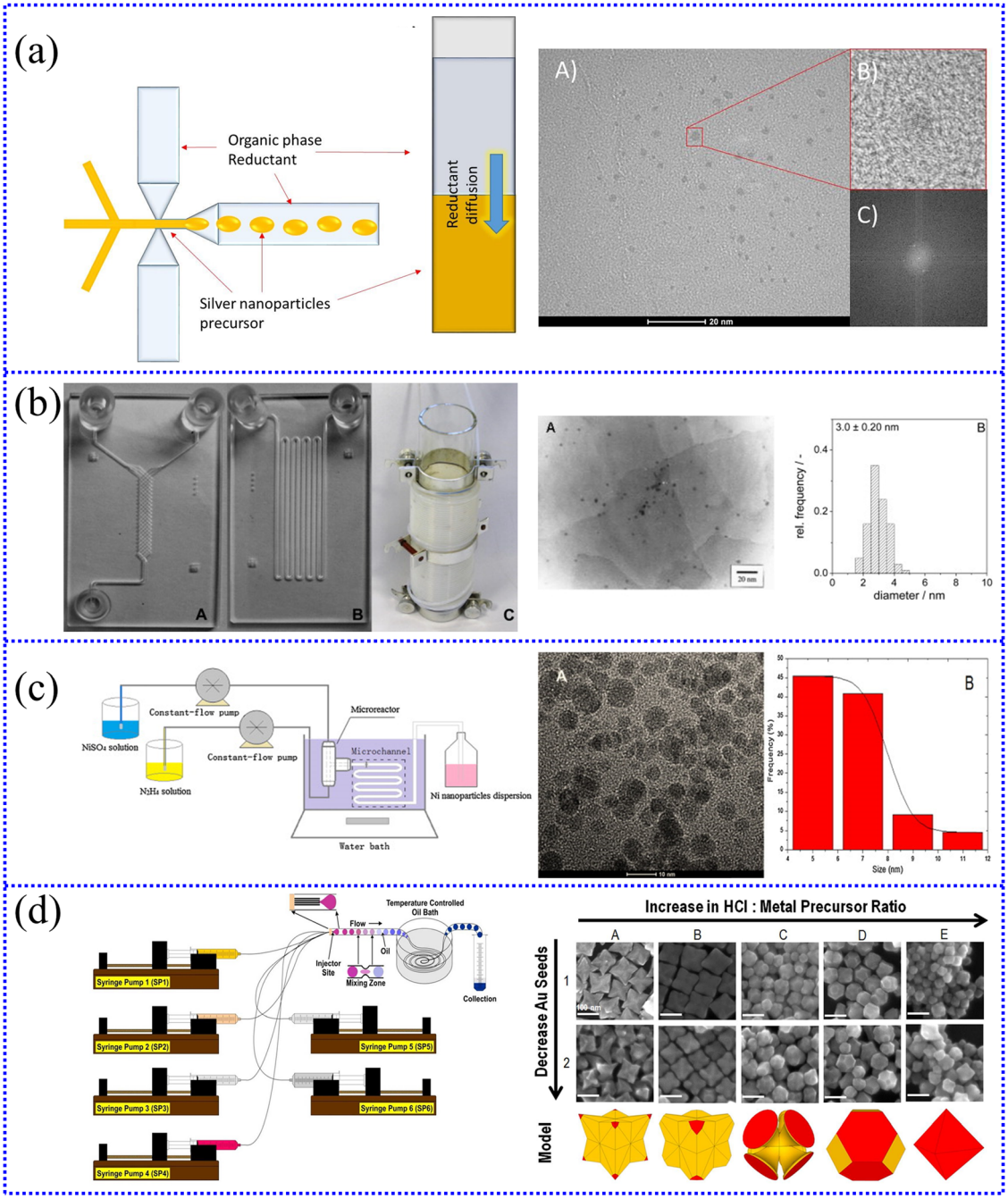

Fig. 12 (a) Ag nanoparticles with a hexagonal structure synthesized in a continuous-flow two-phase microdroplet system.[138] Copyright 2020, Elsevier. (b) Three special microreactors for the synthesis of 1–4 nm Pt nanoparticles.[139] Copyright 2013 Elsevier. (c) Ni nanoparticles with an FCC structure synthesized by employing a T-shaped continuous flow microreactor.[142] Copyright 2015, Elsevier. (d) Au–Pd nanoparticles with various shapes, such as sharp-branched octopods and core@shell octahedra, synthesized in a continuous-flow droplet reactor.[146] Copyright 2018, Royal Society of Chemistry.

state of the two metals).[143–145] Santana *et al.*[146] from Indiana University in the USA reported various methods for synthesizing bimetallic nanoparticles. First, they synthesized Au–Pd nanoparticles with various shapes, such as sharp-branched octopods and core@shell octahedra, using a continuous-flow droplet reactor in the presence of capping agent cetyltrimethylammonium bromide (CTAB) and reducing agent L-ascorbic acid (L-aa), as shown in Fig. 12(d). Six syringes are placed on six syringe pumps during sample preparation through silica capillaries into polytetrafluoroethylene (PTFE) tubing at the injector site. This study provides an innovative idea for the shape design of nanomaterials, which differs from traditional methods, that is, the particle morphology can be changed online by adjusting the relative flow of reagents in the microreactor. Second, they have integrated two microreactors to achieve the synthesis of bimetallic nanoparticles under

Table 2 Other metal micro/nanomaterials synthesized by microreactors

Product	Nanoparticle size (nm)	Mixers type	Flow rate (mL min^{-1})	Residence time (s)	Ref
Au@Pd	3–5	Microchannel	6	8	147
Au–Ag	3.5–4.6	Microchannel	200 μL min^{-1}	—	148
Ni	60–114	Caterpillar mixer	8	3.9	149
Pd	3.0–5.2	Microchannel	380 μL min^{-1}	—	150
Pd	4.4	Microchannel	132 mL h^{-1}	—	151
Co	2.0	Microchannel	0.1	18	152

structure control, including branched Pd–Pt and core@shell Pd@Au nanoparticles. Both are achieved by synthesizing Pd nanocubic particles in the first part of the duo-microreactor, which are then used as seeds for Pt or Au deposition. The duo-microreactor uses six syringes connected to PTFE tubing by silica capillaries. This microreactor has the advantage of achieving bimetallic particle architecture, shape and size control, and it is expected to be applied to other bimetallic nanoparticle synthesis systems. Additionally, other metal micro/nanomaterials, such as Au@Pd, Ni, and Pd, have been successfully synthesized by microreactors, as shown in Table 2. In general, it can be observed that microreactors have huge potential advantages in the synthesis of metal micro/nanomaterials and will surely play a key role in future scientific development.

3.1.2. Inorganic nonmetallic micro/nanomaterials. Inorganic nonmetallic micro/nanomaterials have been widely used in structural materials and functional materials owing to their excellent properties, such as biomedicine, aerospace, optoelectronics, environmental protection and building materials.[153–155] However, the process of synthesizing inorganic nonmetallic micro/nanomaterials by conventional methods may be dangerous, complex, and time- and reagent-consuming. Further, external reaction parameters must also be considered because they play a key role in the uniform reaction for the fine synthesis of micro/nanomaterials. The microreactor structure has been proposed as an innovative engineering tool that provides a fluidic network for creating a large-scale synthesis of nanoparticles, and it is widely used in various industrial and academic fields.

As a key component in the application field of inorganic nonmetallic micro/nanomaterials, semiconductors possess tunable physicochemical properties, such as optical, electronic and surface properties.[156–158] Quantum dots (QDs) are typical semiconductor nanoparticles, also known as ''artificial atoms'', ''superlattices'', ''superatoms'' or ''quantum dot atoms'', which are used in the fields of electrical, optical, electronic and optical fiber networks. QDs refer to semiconductor nanostructures that trap excitons in three spatial directions usually formed from binary compounds, such as CdSe, zinc sulfide (ZnS), cadmium telluride (CdTe), and cadmium sulfide (CdS).[159,160] To date, there have been many studies on the synthesis of QDs with excellent properties.

Edel *et al.*[161] from Imperial College of Science in the UK synthesized CdS nanoparticles from cadmium nitrate tetrahydrate ($Cd(NO_3)_2{\cdot}4H_2O$) and sodium sulfide (Na_2S) using a continuous flow microreactor. The microfluidic chip has an internal volume of 600 nL and is a bilayer device consisting of a glass/silicon/glass interlayer whose two inlet streams are split into a series of independent multichannel streams (16 splits). The facile synthesis and control of the size and monodispersity of certain nanoparticles are demonstrated using a continuous-flow microreactor, which can overcome the complexity of conventional processes.

Kikkeri *et al.*[162] from Max Planck Inst in Germany established a single-phase microfluidic system based on the Syrris microreactor, which is used to synthesize highly luminescent, surface-functionalized CdSe and CdTe nanoparticles. For the synthesis of functionalized QDs, the traditional batch process requires 250–300 °C, but the microfluidic system only requires 160 °C, which significantly reduces the difficulty of the reaction. The lower reaction temperature results in a narrower particle size distribution; herein, the process enables the large-scale, reproducible, and efficient preparation of nanoparticles.

With the cooperation of the South China University of Technology (China), University of California, Santa Cruz (USA), Karlsruhe Institute of Technology (Germany), and Chongqing University (China), Rao *et al.*[163] successfully synthesized nitrogen-doped carbon dots (N-CDs) with a photoluminescence quantum yield (PLQY) of 73% using copper fibers with different porosities to construct a porous copper fiber microreactor, as shown in Fig. 13(a). The optimal process conditions for synthesis are a reaction temperature of 210 °C, a flow rate of 20 mL min^{-1}, an ethylenediamine (EDA) dosage of 1.0 mL, and a copper fiber porosity of 98%. The addition of copper fibers doubles the PLQY of nanoparticles. The discovery of zero-dimensional carbonaceous nanostructures known as carbon dots (CDs) and their unique properties related to fluorescence, quantum confinement and size effects has attracted the interest of researchers.

Hebbar *et al.*[164] from Manipal Acad Higher Educ in India outlined the enhancement of CD synthesis, characterization, application in pollutant detection and photocatalysis, and potential areas for improvement by adding natural carbon precursors or developing microreactor-based techniques.

Perovskite, which emerged in 2012, is called the next-generation quantum dot material.[165–167] It generally refers to a material described by the formula ABX_3, where X is an anion and A and B are cations of different sizes (A is larger than B).[168,169] There have been several related reports on the synthesis of perovskite QDs by microreactors.

With the cooperation of Inha University (Korea), Ajou University (Korea), Kyung Hee University (Korea), and Georgia Institute of Technology (USA), Kang *et al.*[170] successfully synthesized $CsPbX_3$ perovskite nanocrystals with a mean particle diameter of 8.60 ± 0.72 nm, integrating two microfluidic reactors and heating blocks into a microfluidic operating system in series, as shown in Fig. 13(b). The as-synthesized $CsPbBr_3$ nanoparticles are monodisperse with cubic structure and high crystallinity with a lattice distance of ~0.58 nm, which are usually formed by regular self-assembled aggregates. The microfluidic system has the advantages of a large specific surface area, a high mixing and mass transfer rate, and simple operation. Herein, it can be used to finely control anion

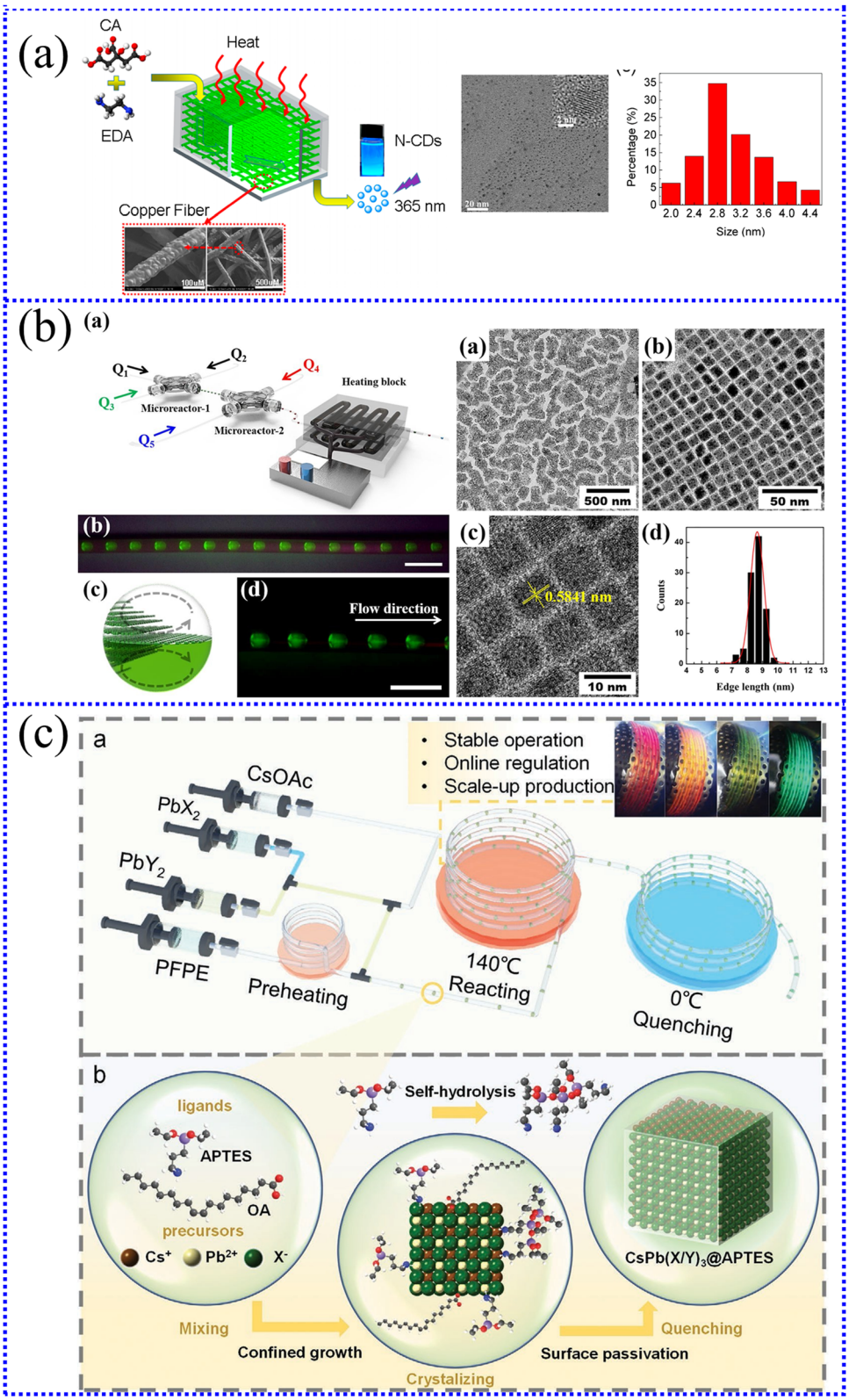

Fig. 13 (a) Porous copper fiber microreactor and synthesized N-CDs.[163] Copyright 2018, MDPI. (b) Microfluidic operating system and 8.60 ± 0.72 nm $CsPbX_3$ perovskite QDs.[170] Copyright 2020, Elsevier. (c) DBMS and $CsPbX_3$@APTES nanocrystals.[172] Copyright 2022, Wiley.

exchange reactions and has great application potential in the large-scale production of perovskite QDs.

Geng *et al.*[171,172] from Tsinghua University in China have conducted many studies on the synthesis of cesium lead halide

perovskite (CHLP) nanocrystals. However, they have systematically prepared $CsPbCl_3$ (9.0 ± 1.0 nm), $CsPbBr_3$ (8.0 ± 1.0 nm), and $CsPbI_3$ (13.0 ± 1.5 nm) nanoparticles based on a droplet microreactor, whose nucleation and growth processes can be precisely controlled within a range of 130 nL. $CsPbBr_3$ nanoparticles synthesized based on this system have a high PLQY of up to 87%, which is far superior to nanocrystals synthesized by other microfluidic systems. Compared with traditional synthetic methods, microreactor-based technology can increase the concentration of reactant precursors by 3–116 times while reducing the ratio of ligand to reactant to as low as 2–50% and improving the theoretical yield of single reaction 2–61.5 times. They also proposed solutions to the problems faced in the development of cesium lead halide perovskite (CHLP) nanocrystals, which greatly promote the industrial development of perovskite nanocrystals. First, an efficient droplet-based microreactor system (DBMS) is designed by ligand engineering to complete the scale-up production of CLHP nanocrystals and obtain 0.26 g high-purity nanocrystal powders (reaction temperature: 140 °C, residence time: 8.26 s), as shown in Fig. 13(c). Second, using 3-aminopropyl triethoxysilane (APTES) as a basic ligand, CLHP nanocrystals that are stable in polar solvents, air environments, and high temperatures are synthesized. The results show that the special Si–O–Si protective layer inhibits the anion exchange between $CsPbBr_3$ and $CsPbI_3$, so the PLQY of $CsPbBr_3$@APTES can be stabilized above 90% for no less than 10 days. Finally, $CsPbX_3$@APTES nanocrystals are fabricated into full-spectrum quantum light-emitting diode (QLED) beads, whose gamut includes 140% of the NTSC color gamut standard.

Recently, magnetic nanoparticles (NPs) have been widely explored owing to their unique magnetic properties in various biological applications, such as bioimaging, drug delivery, and diagnostic ferrofluid hyperthermia, showing a high practical application value.[173,174] Zou *et al.*[175] from East China Normal University (China) provided a new strategy for the controlled synthesis of magnetic nanoparticles (ferroferric oxide, Fe_3O_4) with a size of 17–29 nm using a co-precipitation method *via* a droplet-based continuous microreactor. This chip-type microreactor comprises multifunctional units, in which T-junctions are used for droplet generation; Y-junctions and S-shaped channels are used for droplet fusion and rapid mixing. The prepared Fe_3O_4 nanoparticles have superparamagnetism at room temperature, with maximum saturation magnetization of 61 emu g^{-1} and maximum coercivity of 5.2 Oe.

Several studies on the synthesis of silica (SiO_2) nanoparticles have been reported by Ling *et al.*[176,177] from the University Malaysia Pahang in Malaysia. They synthesized highly monodisperse SiO_2 nanoparticles with an average size of 6 nm in a polydimethylsiloxane microreactor, as shown in Eqn (7) and (8). It is found that the size of the nanoparticles produced by the microreactor is reduced by 93.68% compared with the conventional sol–gel method. They also investigated the effect of residence time on the size of SiO_2 nanoparticles by changing the operating pressure, which affects the flow rate. The results show that by reducing the residence time from 95.65 s to 38.72 s, the size of SiO_2 nanoparticles is reduced from 5.76 nm to 4.89 nm, and its size distribution is reduced to 1.11 nm.

Additionally, several studies on the production of barium sulfate ($BaSO_4$) nanoparticles have been reported. Kockmann *et al.*[178] from Albert-Ludwig University of Freiburg in Germany synthesized $BaSO_4$ nanoparticles with a mean particle size of ~100 nm using a T-type silicon micromixer, as shown in eqn (9). It is found that convective mixing and mass transfer determine the nucleation and growth of nanoparticles, controlling the final particle size distribution. Wang *et al.*[179] from Beijing University of Chemical Technology in China successfully prepared $BaSO_4$ nanoparticles with an average particle size of 37 nm and a narrow particle size distribution through a microporous tube-in-tube microchannel reactor (MTMCR) with a high throughput of 9 L min^{-1}. The size of $BaSO_4$ nanoparticles has a great relationship with the flow rate of reactants in the microchannel, and a high flow rate is conducive to the production of small particles. Du *et al.*[180] from Tsinghua University in China controllably prepared $BaSO_4$ nanoparticles with an average size of 40 nm using a membrane dispersion microreactor to generate microbubbles and selecting saturated Na_2SO_4 solution and BaS solution as reactants. With the introduction of microbubbles, mixing performance can be improved by continuously increasing the gas flow. Yang *et al.*[181] from Hunan University in China prepared $BaSO_4$ nanoparticles with an average particle size of 26 nm using a high-throughput (105.5 g h^{-1}) passive four-stage asymmetric oscillatory feedback microreactor constructed and a chaotic mixing mechanism. Furthermore, other inorganic nonmetallic micro/nanomaterials, such as TiO_2, copper chromite ($CuCr_2O_4$), and CdSe, have also been successfully synthesized by microreactors, as shown in Table 3. In summary, it can be observed that microreactors have huge potential advantages in the synthesis of inorganic nonmatallic micro/nanoparticles and will surely play a more important role in the future development of the world.

$$Si(OC_2H_5)_4 + 4H_2O \rightarrow Si(OH)_4 + 4C_2H_5OH \quad (7)$$

$$Si(OH)_4 \rightarrow SiO_2 + H_2O \quad (8)$$

$$H_2SO_4 + BaCl_2 \rightarrow BaSO_4\downarrow + 2HCl \quad (9)$$

3.2. Synthesis of organic micro/nanomaterials

In various fields, specifically the pharmaceutical industry, organic micro/nanomaterials have an important influence and have been reported by numerous studies.[193–195] To date, nanomedicine is widely used in the diagnosis and treatment of diseases, such as infectious diseases, cardiovascular, and cancer.[196,197] Bangham *et al.*[198] from Agricultural Research Council Institute of Animal Physiology Babraham in England first described the synthesis of nanoliposomes in 1965 at Cambridge University; since then, the preparation, characterization and application of nanoliposomes as carriers of drugs and other biologically active substances have developed considerably. Kuribayashi *et al.*[199] from the University of Tokyo in Japan reported the use of electroformation in microfluidic channels to generate nanoliposomes with a unilayer

Table 3 Other inorganic nonmetallic micro/nanomaterials synthesized by microreactors

Product	Nanoparticle size (nm)	Mixers type	Flow rate (mL min^{-1})	Residence time (s)	Ref
TiO_2	<10	Microchannel	80–200 μL min^{-1}	—	182
TiO_2	50–140	Microchannel	—	0.2	183
$CuCr_2O_4$	192–300	Microchannel	25–150 mL h^{-1}	—	184
CdSe	2.8–4.2	Microchannel	0.1	5–10 min	185
CdSe	2.4–2.69	Microchannel	1.5–3.0 μL min^{-1}	250–500	186
CdS	2–3	Microjet reactor	40 g min^{-1}	6 min	187
$BaSO_4$	15–100	T-mixer	0.15–0.25	—	188
$BaSO_4$	300–670	T-shaped microchannel	2	2.16–2.6	189
$BaSO_4$	6–20 μm	Ultrasonic microreactor	0.2 mL min^{-1}	12.5–120	190
SiO_2	88	Micromixer	35 mL h^{-1}	750	191
CeO_2	15	T-mixer	2–20	—	192

morphology with an average diameter of ~12 μm. The microchannel (30 mm × 60 mm × 1 mm) is made of a sheet of polymethylvinylsiloxane sandwiched between two glass plates (30 mm × 40 mm × 0.12–0.55 mm) coated with indium tin oxide (ITO) electrodes. The average width of each channel is 300 μm, and the volume of the channel is about 2.7 μL. With the cooperation of Chuo University (Japan) and Tokyo University of Marine Science and Technology (Japan), Ushiyama *et al.*[200] have produced giant unilamellar vesicles (GUVs) with an average particle size of 25.6–45.4 μm using microfluidic channels. This device can be operated immediately after bonding the monolithic replicated PDMS channel and the plugging tube without local surface treatment or long-term lowering of the oil layer in the microfluidic channel. The stable state of W/O/W droplet generation can be reached in a short time (1–2 min), and the internal liquid volume can be reduced to ~20 μL.

Engineered polymer microparticles (MPs) have emerged as very interesting multifunctional platforms, where the loaded plasmonic particles are potential triggers for drug delivery applications in biomedicine. Solorzano *et al.*[201] from the University of Zaragoza in Spain developed a simple, versatile, and high-yield microfluidic synthesis technique in which hybrid-thermoresponsive Poly(*N*-isopropylacrylamide) (PNIPAm)-based MPs with a mean size of ~400 μm are obtained using an innovative one-step sequential synthesis method. The coaxial capillary microfluidic device is shown in Fig. 14(a), in which the inner and outer capillaries are made of polyetheretherketone (PEEK, hydrophilic) and PTFE (hydrophobic), respectively.

Recently, to improve the solubility of drugs and solve the problems of bioavailability and drug delivery efficiency, optimizing drug particles into nanoscale products is a potential strategy. Kim *et al.*[202] from Tsinghua University in China reported a continuous-flow T-shaped microreactor for the preparation of itraconazole (ITZ) nanoparticles with an average particle size of 130–340 nm by applying an antisolvent precipitation method. The flow rates of the continuous phase and dispersed phase are 10–250 μL min^{-1} and 50 μL min^{-1}, respectively. The microchannel is made of stainless steel, its geometric structure is a typical cross junction, and the intersection diameter of the metal channel is 1.2 mm.

Maity *et al.*[203] from the Indian Institute of Technology Guwahati in India conveniently synthesized ~10 nm sized nearly monodispersed cellulose acetate nanoparticles (CANPs) using a continuous-flow microreactor, as shown in Fig. 14(b). Solution 1 composed of cellulose acetate (CA) and *N*,*N*-dimethylformamide (DMF) enters from the central inlet (flow rate: 0.01 mL min^{-1}), and the anti-solvent water enters from the two side inlets (flow rate: 0.01 mL min^{-1}), thus forming a core-annular flow. Killing experiments of the synthesized CANPs against Gram-negative Pseudomonas aeruginosa species show enhanced bactericidal activity with or without the loading of the external drug (curcumin).

Jaouhari *et al.*[204] from the University Bordeaux in France synthesized tetraphenylethylene (TPE) nanoparticles with an average size of 9 ± 3 nm using a novel Supercritical AntiSolvent process with a microreactor (μSAS), as shown in Fig. 14(c). Tetrahydrofuran (THF) and supercritical carbon dioxide (sc-CO_2) are used as solvent and antisolvent, respectively. The microreactor is made of silicon and heat-resistant glass to withstand the high-pressure conditions (~200 bar) required by the μSAS process, and its outlet is connected to a sapphire tube (inner diameter: 7.3 mm, outer diameter: 1/2 inch, and length = 10 cm).

Additionally, the conventional synthesis methods of most organic materials are dangerous or have low synthesis efficiency, so the application of microreactors can make the synthesis of organic materials safer and faster. Good heat and mass transfer capabilities, combined with ease of scale-up, not only make microreactors the superior choice in many cases but are also often the only option when dealing with highly reactive, short-lived intermediates. Some studies at Kyoto University in Japan have greatly promoted the development of flash chemistry. Yoshida *et al.*[205,206] gave a brief overview of the concept of flash chemistry, which uses microreactors to perform extremely fast reactions in organic synthesis, and can effectively control the formation of dangerous intermediate products. Kim *et al.*[60] have developed a microfluidic technique based on flash chemistry to selectively functionalize iodophenyl carbamates in the ortho position. Their designed CMR is fabricated by thermal bonding of six layers of polyimide film, and its internal volume is 25 nL provided by a rectangular serpentine channel (width 200 μm, height 125 μm, and length 1 mm). With sub-millisecond fast mixing, unwanted anionic Fries rearrangement[207,208] can be bypassed to obtain the desired product before it occurs.

The development of more rigorous and safe polymerization reactions of bio-based monomers is a major topic in the present era. Pérez *et al.*[209] from Normandie University in France reported

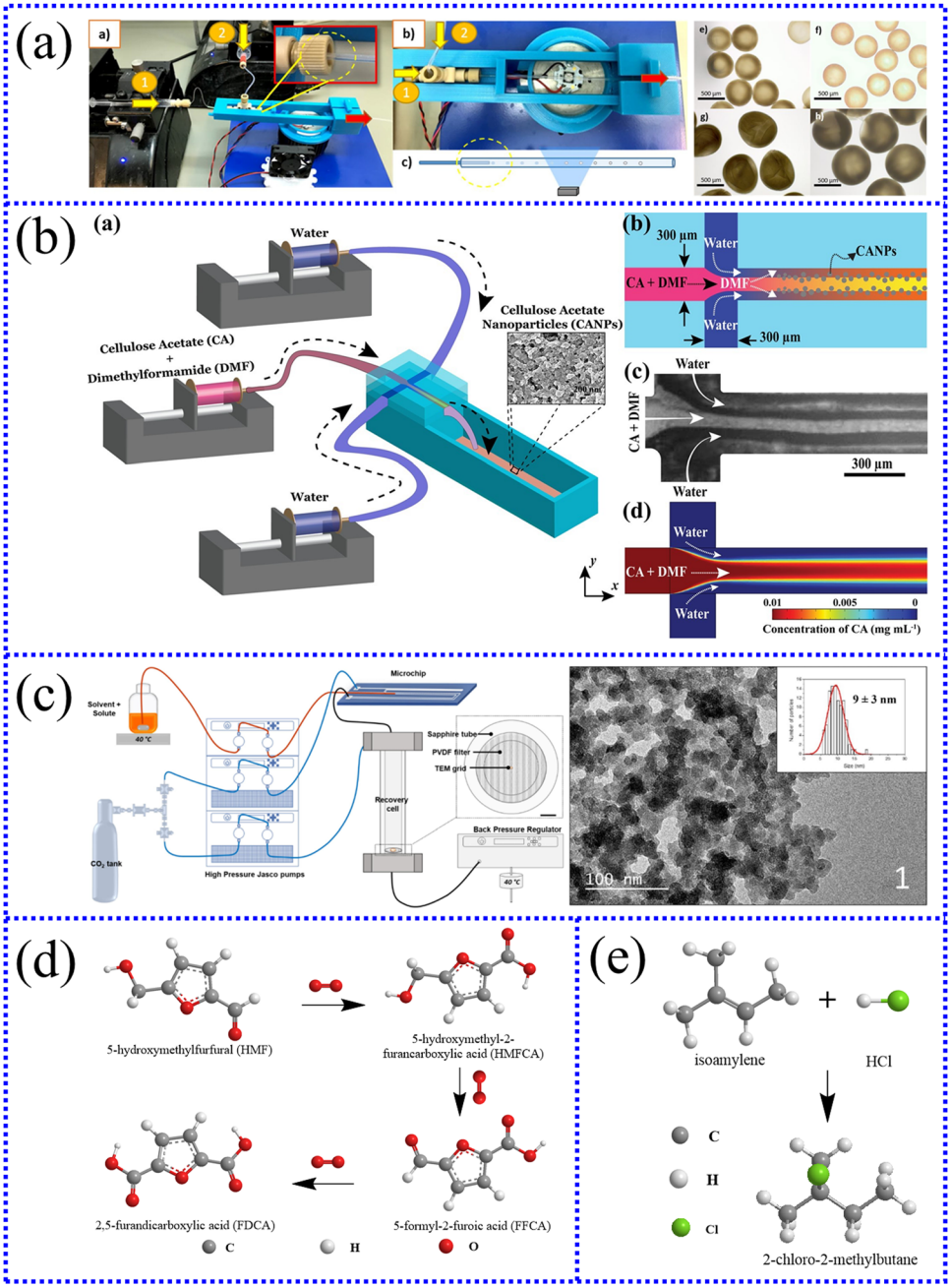

Fig. 14 (a) Coaxial capillary microfluidic device and hybrid-thermoresponsive PNIPAm-based MPs with a mean size of ~400 μm.[201] Copyright 2020, Elsevier. (b) Schematic diagram of the microreactor, the mixing process and the synthesized CNAPs.[203] Copyright 2021, American Chemical Society. (c) Novel supercritical microreactor and TPE nanoparticles with an average size of 9 ± 3 nm.[204] Copyright 2020, Elsevier. (d) Reaction pathway of HMF oxidation to FDCA.[212] (e) Reaction pathway of 2-chloro-2-methylbutane.[213]

the excellent performance of microreactors in finding flexible and sustainable methods for the synthesis of macromolecular scaffolds. It is found that the anionic polymerization of myrcene can be fine-tuned in a microfluidic reactor to produce low molar mass polymyrcene (PMYR). Further, by adding an inlet to the telescoping flow device, it is found that carbon dioxide could be captured, thus introducing carboxylic acid into the PMYR end.

Ozonolysis reactions are generally highly productive, highly selective, and sustainable processes, especially in organic synthesis and chemical manufacturing. However, it has been underutilized owing to safety concerns in handling ozone (O_3) gas and highly reactive ozonide intermediates. Polterauer *et al.*[210] from the University of Graz in Austria explored and optimized the reaction conditions for the ozonation of thioanisole to methyl phenyl sulfoxide and cyclohexene to hexanedial using a dedicated microreactor platform for gas–liquid conversion. The research results show that thioanisole can be converted to methyl phenyl sulfoxide in a 99% yield by

ozonation at 0 °C and <1 s. Similarly, cyclohexene can be converted to hexanedial with a yield of 94% in 1.7 s and 0 °C.

Multinuclear microfluidic double emulsion droplets (DEDs) are excellent microreaction vessels that can encapsulate various reagents and mix them with nuclei coalescence. With the cooperation of China Jiliang University (China), LEO Group Co., Ltd (China), and Jiangsu University (China), Chen *et al.*[211] demonstrated a non-contact strategy for near-infrared (NIR) light to trigger the core coalescence of DEDs. Using a glass capillary microfluidic device, a small amount of Prussian blue (PB) is encapsulated as a photothermal responsive agent to prepare DEDs with dual-core and triple-core. The results show that the coalescence efficiency of this method can reach 98%, demonstrating that NIR light-induced coalescence can open up the possibility of efficient and high-throughput sequential microreactions in chemical analysis, biomedical engineering, and lab-on-a-chip settings.

With the cooperation of Tsinghua University (China), Beijing University of Chemical Technology (China), and SINOPEC Research Institute of Petroleum Processing (China), Yang *et al.*[212] reported that microreactors can significantly accelerate heterogeneous processes, *viz.*, the interaction of gas and liquid phases on solid catalysts. 5-Hydroxymethylfurfural (HMF) is oxidized to 2,5-furandicarboxylic acid (FDCA) as a typical representative of the heterogeneous process, so they tried to use a micropacked-bed reactor (stainless steel, inner diameter: 2 mm) to achieve high-efficiency and ultra-fast continuous-flow synthesis of FDCA, as shown in Fig. 14(d). Au/CeO_2 and O_2 are chosen as catalyst and oxidant, respectively. The HMF conversion and FDCA selectivity can reach 100% and 90% within only 41 s, respectively, indicating that the microreactor significantly improves the gas–liquid mass transfer efficiency, and its space-time yield is 1–2 orders of magnitude higher than that of the conventional reactor.

Xu *et al.*[213] from Wuhan University of Technology in China successfully achieved efficient production of 2-chloro-2-methylbutane with a conversion rate of up to 98.00% using isoamylene and hydrochloric acid as raw materials through a microchannel reactor, as shown in Fig. 14(e). Optimized process conditions: *n* (hydrochloric acid): *n* (isoamylene) = 2.80 : 1.00; isoamylene flow rate, hydrochloric acid flow rate, reaction temperature, pressure and residence time are 1.76 mL min^{-1}, 4.40 mL min^{-1}, 90 °C, 0.70 MPa and 15 min, respectively. The above research results are achieved by effectively increasing the fluid pressure through the back pressure system, which increases the boiling point of isopentene, increases the reaction temperature, and thus increases the reaction rate.

Furthermore, the synthesis of other organic micro/nanomaterials, such as (+)-nootkatone, acetone, and 1-(4-ethoxy-2,3-difluorobenzyl)-4-propylcyclohexan-1-ol, *via* microreactors has been reported in the literature, as shown in Table 4. In conclusion, conventional methods for synthesizing organic micro/nanomaterials face disadvantages, such as a long synthesis time and poor material quality, while microreactors can accelerate the synthesis of organic micro/nanomaterials in a controlled manner and obtain better selectivity and higher yield.

3.3. Synthesis of composite micro/nanomaterials

Composite micro/nanomaterials comprise two or more components or materials, which have many unique properties different from those of individual materials, and are widely used in various fields, including medical diagnosis, construction, and food production.[230–232] The multi-step synthesis capability of microreactors enables fine-tuning of properties, such as particle shape, size, porosity, core/shell structure, and chemical anisotropy, to meet the needs of integrating multiple physical and chemical properties of composite micro/nanomaterials. The doping of various metal and non-metal elements has greatly promoted the development of functional material.[233–235] Thus far, various composite materials, such as organic-based, metal-based, and inorganic non-metallic-based materials, have been successfully produced through microreactors, among which Janus particles and metal–organic frameworks (MOFs) are typical representatives.

3.3.1. Janus particles. As early as 1991, French physicist Pierre-Gilles de Gennes, known as ''contemporary Newton'',

Table 4 Other organic micro/nanomaterials synthesized by microreactors

Product	Yield (%)	Mixers type	Flow rate (mL min^{-1})	Residence time (s)	Ref
Acetone	15	T-shaped mixer	0.03–0.15	0.01–0.08	214
(+)-Nootkatone	20	Microchannel	15 μL min^{-1}	20 min	215
1-(4-Ethoxy-2,3-difluorobenzyl)-4-propylcyclohexan-1-ol	78.1	Membrane dispersion microreactor	8–24	16.3 min	216
1,4-Diphenylbutane	96	T-shaped mixer	12	—	217
1,3,5-Trimethyl-2-nitrobenzene	99.8	Microchannel	39.6	60	218
3,5,5-Trimethylhexanoyl chloride	>99	Microchannel	20	2 min	219
Furfural	92.2	Microchannel	0.05–0.8	15 min	220
Furfural	93	Microchannel	0–5	4 min	221
(*R*)-Cyanohydrins	90–95	Microchannel	0.3	3–30 min	222
Dodecyl benzene Sulfonic acid	99.78	T-shaped mixer	310	—	223
1-Ethoxy-2,3-difluoro-4-iodo-benzene	91.3	Membrane dispersion microreactor	20.8	16 min	224
Neopentyl glycol	96.21	Microchannel	—	2.5 min	225
P-diethynylbenzene	99.2	T-shaped mixer	1	14	226
[OMIM]Br	58.75	T-shaped mixer	0.05–10	4.74 min	227
5-Hydroxymethylfurfural	49	Microchannel	<10	36	228
Piperacillin	94.7	Membrane dispersion microreactor	40	60 min	229

introduced the concept of anisotropic particles with two surface areas in his Nobel Prize lecture, and he named them "Janus particles".[236,237] The asymmetry of Janus particles endows them with various physicochemical and functional properties compared to conventional particles.

Bai *et al.*[238] from the University of Bordeaux in France synthesized Ag@TiO_2 nanoheterodimers (NHDs) with an average diameter range of 8.8–11.9 nm using a laser focused inside a microfluidic reactor, as shown in Fig. 15(a). The chip microreactor comprises two glass channels, one circular channel (with an outer diameter of 550 nm) for nanoparticle solution and the other square channel (with an inner dimension of 600 nm) for oil injection. The final codirectional flow in the square channel is excited by a localized laser. They also found that the growth of individual Ag or Au nanodots can be controlled by varying the beam intensity, the concentration of the metal salt, and the flow rate within the microreactor.

Dobhal *et al.*[239] from the Institute of Chemical Technology in India prepared poly (lactic-*co*-glycolic acid) (PLGA)-encapsulated coumarin-6 nanoparticles on a microreactor continuous platform. Multiple test results show that the nanoparticles are safe to CHO cells (≈80% cell viability) at a concentration of ≤600 μg mL^{-1} and can be successfully absorbed by cells. The effects of the polymer chain length of PLGA and the ratio of lactide to glycyrrhizic acid (LA: GA) on the compatibility of PLGA with coumarin-6 molecules are also explored.

Tofighi *et al.*[240] from the Karlsruhe Institute of Technology (KIT) in Germany continuously synthesized $CuO/ZnO/Al_2O_3$ catalysts by the co-precipitation of metal nitrate aqueous solution and sodium carbonate (Na_2CO_3) in a microfluidic reactor, as shown in eqn (10)–(15). Being made of silicon-bonded glass, the microreactor is specifically designed for *in situ* characterization with X-ray spectroscopy and scattering techniques. The results show that the samples synthesized by mocroreactors are calcined with significantly smaller CuO grains, which enhances the Cu dispersion and active surface area in the final catalyst.

$$2Cu^{2+} + CO_3^{2-} + 2OH^- \rightarrow Cu_2(CO_3)(OH)_2 \quad (10)$$

$$5Zn^{2+} + 2CO_3^{2-} + 6OH^- \rightarrow Zn_5(CO_3)_2(OH)_6 \quad (11)$$

$$2Cu^{2+} + NO_3^{2-} + 3OH^- \rightarrow Cu_2(NO_3)(OH)_3 \quad (12)$$

$$2Cu^{2+} + NO_3^{2-} + 3OH^- \rightarrow Cu_2(NO_3)(OH)_3 \quad (13)$$

$$Cu_2(CO_3)(OH)_3 + Zn^{2+} \rightarrow (Cu_{2-x}Zn_x)(CO_3)(OH)_2 + xCu^{2+} \quad (14)$$

$$Zn_5(CO_3)_2(OH)_6 + xCu^{2+} \rightarrow (Zn_{5-x}Cu_x)(CO_3)_2(OH)_6 + xZn^{2+} \quad (15)$$

Chai *et al.*[241] from Tianjin University in China prepared lignin/chitosan nanoparticles (Lig/Chi NPs) with controllable architecture and a mean size of 180 nm *via* a simple and scalable microreactor setup (*i.e.*, valve-assisted micromixer) and used them for anticancer drug delivery. THF is used as a good solvent for corncob lignin (HGS lignin), and chitosan in an acetic acid aqueous solution is used as an antisolvent. Through electrostatic co-assembly, the amino groups of chitosan and the carboxyl groups of lignin rapidly form Lig/Chi NPs. Anticancer drugs, such as docetaxel (DTX) and curcumin (CCM), are co-assembled with Lig/Chi NPs, which are found to have good drug loading efficiency and biocompatibility. In the acidic solution of the tumor-mimicking microenvironment, the drug release amounts are 51% (DTX@Lig/Chi NPs) and 50% (CCM@Lig/Chi NPs) and have an obvious killing effect on HeLa cells.

Li *et al.*[242] from the Dalian University of Technology in China synthesized a hybrid dye system based on TPE-encapsulated organic dyes, *viz.* aggregation-caused quenching (ACQ)@aggregation-induced emission (AIE)-type nanoparticles (CEAA dyes), using a continuous-flow microreactor, as shown in Fig. 15(b). CEAA nanoparticles can serve as a suitable platform for efficient cascade Förster resonance energy transfer (FRET). The test results show that CEAA dyes have an ultra-efficient light-harvesting ability, which is reflected in the energy transfer efficiency of 99.37%, the antenna effect of 26.23, and the red-shift distance of 126 nm.

Furthermore, to promote the application of microreactors in the synthesis of composite micro/nanomaterials, members of our team, such as Xu *et al.*,[243–245] have conducted several studies. First, they proposed a method for synthesizing Ni–B amorphous nanoparticles with an average particle size of 9 nm by reducing $NiSO_4$ with $NaBH_4$ aqueous solution through a stainless steel micro-mixer. The prepared Ni–B amorphous nanoparticles are spherical and have good dispersion. Second, they synthesized Cu@Cu_2O nanocomposites with a mean particle size of 20–50 nm using $CuSO_4$ and $NaBH_4$ as raw materials at 25 °C in a microreactor. It is found that by controlling the oxidation process, the surface of Cu nanoparticles is oxidized to Cu_2O, forming an open bicontinuous and dimensional

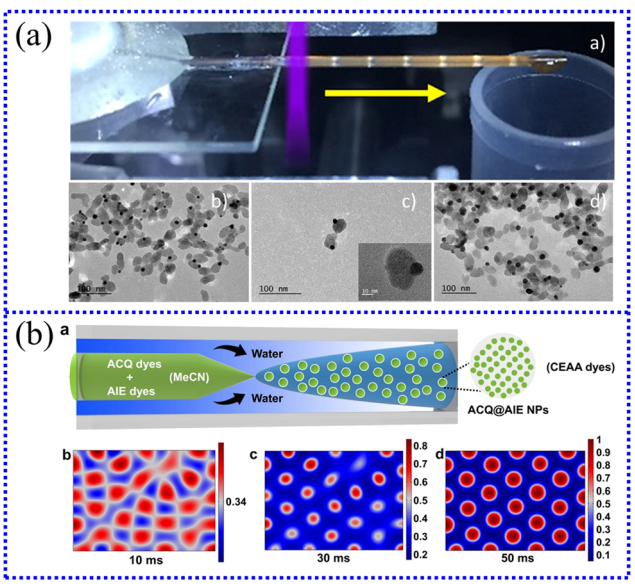

Fig. 15 (a) Laser synthesis of Ag@TiO_2 nanoparticles with an average diameter of 8.8–11.9 nm in a microfluidic reactor.[238] Copyright 2021, American Chemical Society. (b) Continuous-flow microreactor and CEAA dyes.[242] Copyright 2022, Springer Nature.

framework structure. When MB is oxidized in the UV/H_2O_2 system, the addition of Cu@Cu_2O nanocomposites promotes strong oxidizing free radicals, such as $HO^{\bullet}$, $HOO^{\bullet}$, and $O_2^{\bullet -}$ to be generated in large quantities, so the highest oxidation efficiency reaches 96.5%. Third, they synthesized Cu–Cuo nanocomposites with a grain size of 10 nm using a microreactor to controlly oxidize Cu nanoparticles prepared using the liquid phase reduction method. The microreactor is made of stainless steel with a channel width of 40 μm. The Cu–CuO nanocomposite has good catalytic activity when photodegrading composite H_2O_2 to oxidize methylene blue (MB), and the total degradation rate can reach 98.5% after 50 min of reaction. In summary, microreactors have outstanding advantages in the production of Janus particles and will surely play a more important role in the synthesis of special materials in the future.

3.3.2. Metal–organic frameworks. MOFs are a class of multifunctional composite porous crystalline materials in which organic ligands and inorganic metal centers are connected by self-assembly, which can be used as gas storage and separation, catalysts for organic transformations, biomedicine, sensors, photovoltaics and energy conversion.[246–248] However, conventional MOFs are synthesized by time-consuming hydrothermal or solvothermal methods, which generally require hours or days for the crystallization and formation of porous networks. Droplet-based microfluidic devices have a high surface-to-volume ratio, efficient mixing and heat transfer efficiency and can eliminate channel blockage and significantly increase the reaction rate; thus, they are widely used in high-throughput biological and biochemical screening experiments.

With the cooperation of Pohang University of Science and Technology (Korea), Inha University (Korea), and Ulsan National Institute of Science and Technology (UNIST, Korea), Faustini *et al.*[249] continuously and ultrafastly synthesized homogeneous MOFs (*i.e.*, HKUST-1, MOF-5, IRMOF-3 and UiO-66) and core–shell MOFs (*i.e.*, Co_3BTC_2@Ni_3BTC_2, MOF-5@diCH_3-MOF-5 and Fe_3O_4@ZIF-8) based on the microfluidic strategy of nanoliter droplets, as shown in Fig. 16(a). The microreactor is a T-shaped junction PDMS chip device prepared using the simple one-step scaffolding method of microfluidics. Its special structure allows a simple and direct connection between the droplet generating device and the perfluoroalkoxyalkane (PFA) tubing, thus preventing droplet leakage and merging. Compared with conventional hydrothermal and solvothermal synthesis methods, the morphology of MOFs synthesized based on microfluidic technology is more uniform.

Chen *et al.*[250] from Virginia Commonwealth University in the USA developed a microdroplet-based synthesis process for MOFs with short and scalable processing times. The formation of copper 1,4-benzenedicarboxylate (CuBDC) MOF under changing flow conditions by adjusting the operating pressure is investigated. When the operating pressure is reduced, the spray system transitions to a state of free molecular flow. The transport phenomenon of micro-droplets becomes obvious owing to the dispersion of the surrounding gas, thus making the formed MOFs have unique morphological and structural characteristics.

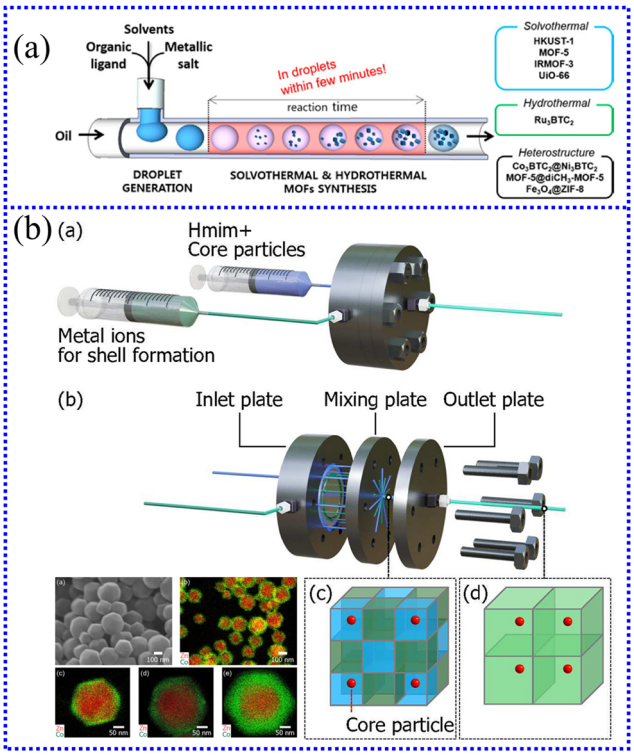

Fig. 16 (a) Homogeneous MOFs and core–shell MOFs synthesized using the microfluidic strategy.[249] Copyright 2013, American Chemical Society. (b) Zeolite imidazolate frameworks-8 (ZIF-8)@ZIF-67 and ZIF-67@ZIF-8 core–shell particles synthesized using microreactor.[251] Copyright 2021, American Chemical Society.

In addition, MOFs with a core–shell structure can enhance the intrinsic properties of constituent MOFs and endow additional functional activities. The microreactor can ensure good mixing and control the thickness of the shell layer, which provides the possibility of adjusting the particle characteristics of core–shell MOF. Fujiwara *et al.*[251] from Kyoto University in Japan synthesized zeolite imidazolate frameworks-8 (ZIF-8)@ZIF-67 and ZIF-67@ZIF-8 core–shell particles with a shell thickness range of 32–66 nm *via* a microreactor, and they investigated the effect of mixing properties on the shell thickness of the obtained particles. The microreactor comprises the inlet, mixing plate and outlet plate; the reactants are injected into it at a flow rate of 10 mL min^{-1}, as shown in Fig. 16(b). Their results confirm that rapid mixing is critical for the homogeneity of the synthesized particles. In addition, this synthetic method also facilitates the preparation of ZIF-8@ZIF-67@ZIF-8@ZIF-67 multilayered particles.

Furthermore, owing to their highly anisotropic and tunable chemical composition, two-dimensional (2D) MOFs have great potential as building blocks for next-generation materials in various applications, ranging from electrochemical catalysis to membrane separation.

Several studies at the University of Cambridge in the UK have greatly promoted the development of MOFs.[252,253] However, they prepared CuBDC nanosheets with a side length in the range of 30–40 nm using a high-shear annular microreactor

Table 5 Other composite micro/nanomaterials synthesized by microreactors

Product	Nanoparticle size (nm)	Mixers type	Flow rate (mL min^{-1})	Residence time (s)	Ref
CdSe–ZnS	—	Microchannel	100 μL min^{-1}	2.0–2.7	254
UIO-66	80–110	Microchannel	0.2	1.1 min	255
ZIF-8	50 nm–2 μm	Microchannel	10	—	256
CPO-27-Ni	40	Microchannel	1	20 min	257
α-NaYF4:Yb,Er	6.1–13.4	Microchannel	100 μL min^{-1}	8–9 min	258
FDCANi	—	Tubular microreactor	10	15 ms	259
POSS	~5 μm	Microchannel	15–90 μL min^{-1}	—	260
YVO4:Eu	84–103	Microchannel	3–8	7–18	261
M/TiO_2 (M = Pd, Pt or Au)	3.0–4.2	Cross-shaped micromixer	0.2	2 min	262

and investigated the effect of different solvent environments on their structure and aggregation kinetics. Using liquid cell transmission electron microscopy (LCTEM), it is found that 2D MOF nanosheets have directional attachment, and the growth rate and direction are controlled by solvent-surface interactions. Moreover, they developed a new method for the synthesis of 2D CuBDC with a side length of approximately 37 nm and a thickness of <1 nm at room temperature using high-shear annular microreactor technology. The microreactor belongs to an annular structure, in which three quartz tubes are installed in a ''tube-in-tube'' structure to form two annular flow zones. The space-time yield of CuBDC in a microreactor is found to be five orders of magnitude higher than that in a batch reactor. Furthermore, other composite micro/nanomaterials, such as YVO4:Eu, CdSe–ZnS, and UIO-66, have also been successfully synthesized by microreactors, as shown in Table 5. In summary, the microreactor has significant advantages in the synthesis of MOFs, which will surely play an important role in the diversified development of functional materials in the future.

4. Conclusions and outlook

Microreactors and continuous flow chemical reactions are increasingly accepted in many fields and applied in all aspects of people's lives in a flexible and controllable manner. This review describes the fabrication and design principles of microreactors and shows excellent adaptability in the processing and synthesis of micro/nanomaterials, including metal nanoparticles, inorganic nonmetallic nanoparticles, organic nanoparticles, Janus particles, and MOFs. Therefore, microreactors are effective platforms for the synthesis of micro/nanomaterials. Specifically, microreactors can operate on the concept of small surface areas, which means that the frequency of molecular collisions is kinetically and significantly increased, ultimately speeding up the production of products. Thus far, microreactor technology has successfully solved some of the problems faced by industrial large-scale production of synthetic materials or chemicals. However, there are still some deficiencies and improvement measures in the field of the synthesis of micro/nanomaterials based on microreactors:

(i) The fluid in the microreactor is usually in a laminar flow state, so it is significantly affected by surface tension, resulting in a relatively slow mixing mass transfer rate, and is easy to be blocked. The most effective way to solve these problems is to introduce external fields (*i.e.*, electric fields, electromagnetic fields, ultrasonic fields, and supergravity) or design the internal channel of the microreactor into a special structure. Some studies conducted at Katholieke Universiteit Leuven (Belgium), University of Twente (Netherlands), Amirkabir University of Technology (Iran), and Dalian Institute of Chemical Physics (China) have been reported.[263–265] Furthermore, to optimize the microreactor design and processing cost when synthesizing special nanoparticles, many studies have made related reports. With the cooperation of the University of Southampton (UK) and the University of Oviedo (Spain), Cristaldi *et al.*[266] developed a significantly more cost-effective and easy-to-execute fabrication method for microreactors. Notably, they also tested the operation of the microreactor at a wide range of volumetric flow rates (up to 20 mL min^{-1}). Studies have shown that this process can make the production time (from design to finished product) less than 1 day, and the average material cost is ~£5, which is very suitable for large-scale production of microreactors. Nandiwale *et al.*[267] from the Massachusetts Institute of Technology in the USA proposed a continuous stirred tank reactor (CSTR) cascade that can handle slurry/solids during in-flow chemical conversion by combining 3D printing of a master mold with the sealing of PDMS channel replicas using pressure-sensitive tape.

(ii) Integrating multifunctional nanomaterials into microreactors can achieve more functions and improve their performance in various applications, such as efficient hydrogenation, drug delivery, and photoelectron transfer. Merino-Garcia *et al.*[268] from Universidad de Cantabria in Spain proposed the application of $Cu_2O/Mo_2C/TiO_2$ heterostructures in optofluidic microreactors to convert CO_2 into methanol through a continuous visible light drive. The results show that the yield and apparent quantum yield of methanol reached 36.3 μmol g^{-1} h^{-1} and 0.64%, respectively, and the reaction selectivity is 0.93. This can be attributed to the role of Cu_2O in the selectivity of the reaction to methanol. With the cooperation of the Technical University of Denmark (Denmark), Wuhan Textile University (China), South China University of Technology (China), and Henan University of Engineering (China), Zuo *et al.*[269] first encapsulate FeOCl in a MOF as a yolk–shell reactor (FeOCl-MOF) *via in situ* growth. The interaction of FeOCl with MOF considerably enhanced the effective conversion of H_2O_2 and

•OH utilization (from 25.5% (Fe^{2+}/H_2O_2) to 77.1% (FeOCl-MOF/H_2O_2).

(iii) The theory of material synthesis under micro-scale effects needs to be further studied, such as viscoelastic properties, residual stress, and micro-damage. A more solid foundation needs to be laid for scientific design and rational manufacturing. Additionally, the *in situ* detection technology at the micro-scale urgently needs to be innovated and improved. Thus far, effective detection methods are still scarce. A more detailed understanding of the formation process of micro/nanomaterials will help to further promote their high-quality development.

(iv) The most special thing is that the micro/nano materials synthesized using microreactors often show better performance than materials prepared using traditional production methods. However, most developing countries have limited resources for high-end facilities, thus hampering the commercialization of several advanced microreactor processing technologies. More relevant processes need to be reported on the performance optimization of the whole system to make large-scale integrated microreactors more feasible. Overall, more researchers should adapt their efforts from theoretical testing to commercial applications during the synthesis of micro/nanomaterials in microreactors. Given the rapid pace of development in this field, various intertwined development routes of science and technology can be observed, which can obviously further expand the application field of microreactors.

Author contributions

Jianfeng Ran: writing – original draft and investigation. Xuxu Wang: writing – original draft. Yuanhong Liu: discussion and writing – review and editing. Shaohua Yin, Shiwei Li and Libo Zhang: supervision and funding.

Abbreviations

mTAS	Micro total analysis systems
MEMS	Micro electro mechanical systems
IMM	Institute of Microtechnique Mainz
DICP	Dalian Institute of Chemical Physics
ECUST	East China University of Science and Technology
CAGR	Compound annual growth rate
LIGA	Lithography, galvanoformung and abformung
EDM	Electro-discharge machining
DNA	Deoxyribonucleic acid
PDMS	Polydimethylsiloxane
3D	Three dimensional
CBN	Cubic boron nitride
TMAH	Tetramethyl ammonium hydroxide
KOH	Potassium hydroxide
HF	Hydrofluoric acid
HNO_3	Nitric acid
UNIMAS	Universiti Malaysia Sarawak
CFD	Computational fluid dynamics
Re	Reynolds numbers
SHM	Staggered herringbone mixer
Au	Gold
Ag	Silver
Cu	Copper
Pt	Platinum
Pd	Palladium
PVP	Polyvinyl pyrrolidone
$AgNO_3$	Silver nitrate
$NaBH_4$	Sodium borohydride
TiO_2	Titanium oxide
CdSe	Cadmium selenide
Pe	Peclet number
$CuSO_4$	Copper sulfate
FCC	Face-centered cubic
$NiSO_4$	Nickel sulfate
N_2H_4	Hydrazine
CTAB	Cetyltrimethylammonium bromide
L-aa	L-ascorbic acid
PTFE	Polytetrafluoroethylene
QDs	Quantum dot
ZnS	Zinc sulfide
CdTe	Cadmium telluride
CdS	Cadmium sulfide
$Cd(NO_3)_2{\cdot}4H_2O$	Cadmium nitrate tetrahydrate
Na_2S	Sodium sulfide
N-CDs	Nitrogen-doped carbon dots
PLQY	Photoluminescence quantum yield
EDA	Ethylenediamine
CDs	Carbon dot
CHLP	Cesium lead halide perovskite
DBMS	Droplet-based microreactor system
APTES	Aminopropyl triethoxysilane
QLED	Quantum light-emitting diode
NPs	Nanoparticles
Fe_3O_4	Ferroferric oxide
SiO_2	Silica
$BaSO_4$	Barium sulfate
MTMCR	Microporous tube-in-tube microchannel reactor
$CuCr_2O_4$	Copper chromite
ITO	Indium tin oxide
GUVs	Giant unilamellar vesicles
MPs	Microparticles
PNIPAm	Poly(*N*-isopropylacrylamide)
PEEK	Polyetheretherketone
ITZ	Itraconazole
CANPs	Cellulose acetate nanoparticles
CA	Cellulose acetate
DMF	*N*,*N*-dimethylformamide
TPE	Tetraphenylethylene
μSAS	Supercritical AntiSolvent process with microreactor
THF	Tetrahydrofuran
sc-CO_2	Supercritical carbon dioxide

CMR	Chip microreactor
PMYR	Polymyrcene
O_3	Ozone
DEDs	Double emulsion droplets
NIR	Near-infrared
PB	Prussian blue
HMF	5-Hydroxymethylfurfural
FDCA	2,5-Furandicarboxylic acid
MOFs	Metal–organic frameworks
NHDs	Nanoheterodimers
PLGA	Poly (lactic-*co*-glycolic acid)
LA : GA	The ratio of lactide to glycyrrhizic acid
KIT	Karlsruhe Institute of Technology
Na_2CO_3	Sodium carbonate
Lig/Chi NPs	Lignin/chitosan nanoparticles
DTX	Docetaxel
CCM	Curcumin
ACQ	Aggregation-caused quenching
AIE	Aggregation-induced emission
CEAA	ACQ@ AIE-type nanoparticles
FRET	Förster resonance energy transfer
MB	Methylene blue
PFA	Perfluoroalkoxyalkane
CuBDC	Copper benzene dicarboxylic acid
ZIF	Zeolite imidazolate frameworks
LCTEM	Liquid cell transmission electron microscopy
2D	Two-dimensional
CSTR	Continuous stirred tank reactor

Conflicts of interest

The authors declare that they have no known competing financial interests or personal relationships that could have appeared to influence the work reported in this paper.

Acknowledgements

Financial support from the following programs is gratefully acknowledged: National Natural Science Foundation of China (Grant No. 52264051) and Yunnan Ten Thousand Talents Plan Young & Elite Talents Project (Grant No. YNWR-QNBJ-2018-323).

References

1 D. Chen, Y. Wang, H. Zhou, Z. Huang, Y. Zhang, C. F. Guo and H. Zhou, *Adv. Mater.*, 2022, 2200903.
2 L.-L. Li, H.-W. An, B. Peng, R. Zheng and H. Wang, *Mater. Horiz.*, 2019, **6**, 1794–1811.
3 K. Ariga, Q. Ji, W. Nakanishi, J. P. Hill and M. Aono, *Mater. Horiz.*, 2015, **2**, 406–413.
4 B. Xia, Y. Yan, X. Wang and X. W. D. Lou, *Mater. Horiz.*, 2014, **1**, 379–399.
5 C. Li, O. J. H. Chai, Q. Yao, Z. Liu, L. Wang, H. Wang and J. Xie, *Mater. Horiz.*, 2021, **8**, 1657–1682.
6 R. D. Rodriguez, A. Khalelov, P. S. Postnikov, A. Lipovka, E. Dorozhko, I. Amin, G. V. Murastov, J.-J. Chen, W. Sheng and M. E. Trusova, *Mater. Horiz.*, 2020, **7**, 1030–1041.
7 B. M. R. Guimarães, M. V. Scatolino, M. A. Martins, S. R. Ferreira, L. M. Mendes, J. T. Lima, M. G. Junior and G. H. D. Tonoli, *Environ. Sci. Pollut. Res.*, 2022, **29**, 8665–8683.
8 M. Zeng, M. Chen, D. Huang, S. Lei, X. Zhang, L. Wang and Z. Cheng, *Mater. Horiz.*, 2021, **8**, 758–802.
9 A. Kumar, A.-J. Ahmed, O. Bazaka, E. P. Ivanova, I. Levchenko, K. Bazaka and M. V. Jacob, *Mater. Horiz.*, 2021, **8**, 3201–3238.
10 M. Bally and J. Vörös, *Nanomedicine*, 2009, **4**, 447–467.
11 N. J. Wittenberg and C. L. Haynes, *Wiley Interdiscip. Rev.: Nanomed. Nanobiotechnol.*, 2009, **1**, 237–254.
12 Q.-Y. Zhou, C. Fan, C. Li, Y.-L. Wang, Z.-Q. Chen, Q. Yu and M.-Q. Zhu, *Mater. Horiz.*, 2018, **5**, 474–479.
13 A. Yan and Z. Chen, *Int. J. Mol. Sci.*, 2019, **20**, 1003.
14 A. Barhoum, J. Jeevanandam, A. Rastogi, P. Samyn, Y. Boluk, A. Dufresne, M. K. Danquah and M. Bechelany, *Nanoscale*, 2020, **12**, 22845–22890.
15 G.-H. Lee, Y.-S. Kim, E. Kwon, J.-W. Yun and B.-C. Kang, *Pharmaceutics*, 2020, **12**, 826.
16 Y. Y. Khine and M. H. Stenzel, *Mater. Horiz.*, 2020, **7**, 1727–1758.
17 B. L. Li, R. Li, H. L. Zou, K. Ariga, N. B. Li and D. T. Leong, *Mater. Horiz.*, 2020, **7**, 455–469.
18 L. D. Blackman, T. D. Sutherland, P. J. De Barro, H. Thissen and K. E. Locock, *Mater. Horiz.*, 2022, **9**, 2076–2096.
19 M. Heckele and W. Schomburg, *J. Micromech. Microeng.*, 2003, **14**, R1.
20 A. K. Sahu, J. Malhotra and S. Jha, *Opt. Laser Technol.*, 2022, **146**, 107554.
21 M. Protière, N. Nerambourg, O. Renard and P. Reiss, *Nanoscale Res. Lett.*, 2011, **6**, 1–14.
22 T. Kim, S. W. Kim, M. Kang and S.-W. Kim, *J. Phys. Chem. Lett.*, 2012, **3**, 214–218.
23 G. M. Whitesides, *Nature*, 2006, **442**, 368–373.
24 D. E. Fitzpatrick, C. Battilocchio and S. V. Ley, *ACS Cent. Sci.*, 2016, **2**, 131–138.
25 H. J. Lee, R. C. Roberts, D. J. Im, S. J. Yim, H. Kim, J. T. Kim and D. P. Kim, *Small*, 2019, **15**, 1905005.
26 E. Y. Erdem, J. C. Cheng, F. M. Doyle and A. P. Pisano, *Small*, 2014, **10**, 1076–1080.
27 P. L. Suryawanshi, S. P. Gumfekar, B. A. Bhanvase, S. H. Sonawane and M. S. Pimplapure, *Chem. Eng.*, 2018, **189**, 431–448.
28 D. R. Mokoena, B. P. George and H. Abrahamse, *Int. J. Mol. Sci.*, 2019, **20**, 4771.
29 R. P. Feynman, Plenty of Room at the Bottom, APS Annual Meeting, 1959.
30 W. Reschetilowski, *Microreactors in preparative chemistry: practical aspects in bioprocessing, nanotechnology, catalysis and more*, John Wiley & Sons, 2013.
31 L. Licklider and W. G. Kuhr, *Anal. Chem.*, 1994, **66**, 4400–4407.

32 Y. Liu, X. Liu, S. Yang, F. Li, C. Shen, M. Huang, J. Li, R. R. Nasaruddin and J. Xie, *ACS Sustainable Chem. Eng.*, 2018, **6**, 15425–15433.
33 F. Liguori and P. Barbaro, *J. Catal.*, 2014, **311**, 212–220.
34 Q. Zhang, R. J. Somerville, L. Chen, Y. Yu, Z. Fei, S. Wang, P. J. Dyson and D. Min, *J. Hazard. Mater.*, 2023, **443**, 130270.
35 T. Schwalbe, V. Autze and G. Wille, *Chimia*, 2002, **56**, 636.
36 P. Watts and S. J. Haswell, *Chem. Soc. Rev.*, 2005, **34**, 235–246.
37 A. Dellaquila, C. Le Bao, D. Letourneur and T. Simon-Yarza, *Adv. Sci.*, 2021, **8**, 2100798.
38 N.-T. Nguyen and Z. Wu, *J. Micromech. Microeng.*, 2004, **15**, R1.
39 V. Hessel, H. Löwe and F. Schönfeld, *Chem. Eng. Sci.*, 2005, **60**, 2479–2501.
40 Z. Wen, X. Yu, S.-T. Tu, J. Yan and E. Dahlquist, *Bioresour. Technol.*, 2009, **100**, 3054–3060.
41 V. Hessel, C. Knobloch and H. Lowe, *Recent Pat. Chem. Eng.*, 2008, **1**, 1–16.
42 I. Dencic, V. Hessel, M. H. de Croon, J. Meuldijk, C. W. van der Doelen and K. Koch, *ChemSusChem*, 2012, **5**, 232–245.
43 A. A. Bojang and H.-S. Wu, Design, fundamental principles of fabrication and applications of microreactors, *Processes*, 2020, **8**(8), 891.
44 L. R. Volpatti and A. K. Yetisen, *Trends Biotechnol.*, 2014, **32**, 347–350.
45 I. Baumann and P. Westermann, *BioMed Res. Int.*, 2016, **2016**, 8469357–8469372.
46 Y. Asanomi, H. Yamaguchi, M. Miyazaki and H. Maeda, *Molecules*, 2011, **16**, 6041–6059.
47 H. G. Jolliffe and D. I. Gerogiorgis, *Chem. Eng. Res. Des.*, 2015, **97**, 175–191.
48 I. Rossetti and M. Compagnoni, *Chem. Eng. J.*, 2016, **296**, 56–70.
49 K. K. Gill, R. Gibson, K. H. C. Yiu, P. Hester and N. M. Reis, *Chem. Eng. J.*, 2021, **408**, 127860.
50 D. Obino, M. Vassalli, A. Franceschi, A. Alessandrini, P. Facci and F. Viti, *Sensors*, 2021, **21**, 3058.
51 A. Zizzari, M. Bianco, L. Carbone, E. Perrone, F. Amato, G. Maruccio, F. Rendina and V. Arima, *Materials*, 2017, **10**, 1411.
52 D. F. Odetade and G. T. Vladisavljević, *Micromachines*, 2016, **7**, 236.
53 K. K. Saxena, J. Qian and D. Reynaerts, *Int. J.Mach. Tools Manuf.*, 2018, **127**, 28–56.
54 J. C. G. Peres, C. D. C. Herrera, S. L. Baldochi, W. De Rossi and A. Dos Santos Vianna Jr, *The Canadian Journal of Chemical Engineering*, 2019, **97**, 594–603.
55 M. Kuang, L. Wu, Z. Huang, J. Wang, X. Zhang and Y. Song, *ACS Appl. Mater. Interfaces*, 2020, **12**, 30962–30971.
56 A. Beck, F. Obst, M. Busek, S. Grünzner, P. J. Mehner, G. Paschew, D. Appelhans, B. Voit and A. Richter, *Micromachines*, 2020, **11**, 479.
57 N. Mohammad, S. Aravamudhan and D. Kuila, *Nanomaterials*, 2022, **12**, 2425.
58 H. A. Hamid and Z. Çelik-Butler, *Sens. Actuators, A*, 2020, **313**, 112175.
59 S. Bachollet, K. Terao, S. Aida, Y. Nishiyama, K. Kakiuchi and M. Oelgemöller, *Beilstein J. Org. Chem.*, 2013, **9**, 2015–2021.
60 H. Kim, K.-I. Min, K. Inoue, D. J. Im, D.-P. Kim and J.-I. Yoshida, *Science*, 2016, **352**, 691–694.
61 C. Chircov and A. M. Grumezescu, *Micromachines*, 2022, **13**, 164.
62 C. K. Malek and V. Saile, Applications of LIGA technology to precision manufacturing of high-aspect-ratio micro-components and-systems: a review, *Microelectron. J.*, 2004, **35**(2), 131–143.
63 H. Cong and N. Zhang, *Biomicrofluidics*, 2022, **16**, 021301.
64 Y. Miyawaki, Y. Kondo, M. Sekine, K. Ishikawa, T. Hayashi, K. Takeda, H. Kondo, A. Yamazaki, A. Ito and H. Matsumoto, *Jpn. J. Appl. Phys.*, 2012, **52**, 016201.
65 S. Zaki, N. Zhang and M. D. Gilchrist, *Micromachines*, 2022, **13**, 468.
66 X. Huang, L. Li, S. Zhao, L. Tong, Z. Li, Z. Peng, R. Lin, L. Zhou, C. Peng and K.-H. Xue, *Nano-Micro Lett.*, 2022, **14**, 174.
67 K. Takahata, N. Shibaike and H. Guckel, *Microsyst. Technol.*, 2000, **6**, 175–178.
68 B. A. Rizkin, F. G. Popovic and R. L. Hartman, *J. Vac. Sci. Technol., A*, 2019, **37**, 050801.
69 S. M. P. Kalaiselvi, E. Tang, H. Moser, M. Breese, S. P. Turaga, H. Kasi and S. P. Heussler, *Sci. Rep.*, 2022, **12**, 1–12.
70 J. Wang, H. Wang, L. Lai and Y. Li, *Micromachines*, 2020, **12**, 23.
71 C. S. Effenhauser, G. J. Bruin, A. Paulus and M. Ehrat, *Anal.l Chem.*, 1997, **69**, 3451–3457.
72 D. Han, K. Yoshida and J.-W. Kim, *Int. J. Adv. Des. Manuf. Technol.*, 2020, **110**, 3391–3405.
73 D. J. Guckenberger, T. E. De Groot, A. M. Wan, D. J. Beebe and E. W. Young, *Lab Chip*, 2015, **15**, 2364–2378.
74 C.-M. Ho and Y.-C. Tai, *Annu. Rev. Fluid Mech.*, 1998, **30**, 579–612.
75 P. Plouffe, M. Bittel, J. Sieber, D. M. Roberge and A. Macchi, *Chem. Eng. Sci.*, 2016, **143**, 216–225.
76 M. Pileni, *J. Phys. Chem.*, 1993, **97**, 6961–6973.
77 M. J. Madou, *Fundamentals of microfabrication: the science of miniaturization*, CRC press, 2002.
78 T. Masaki, K. Kawata and T. Masuzawa, *Micro electro-discharge machining and its applications, Proceedings of IEEE International workshop on Micro Electro Mechanical Systems*, 1990, pp. 21–26.
79 I. Sabotin, G. Tristo and J. Valentinčič, *Micromachines*, 2020, **11**, 594.
80 K. P. Rajurkar, M. Sundaram and A. Malshe, *Procedia Cirp*, 2013, **6**, 13–26.
81 K. Ishfaq, R. Naveed, M. A. Maqsood and M. Rehman, *Int. J. Adv. Des. Manuf. Technol.*, 2022, 1–18.
82 M. Rahman, Y. Wong and M. Nguyen, Compound and Hybrid Micromachining: Part II-Hybrid Micro-EDM and

Micro-ECM, Comprehensive Materials Processing, 2014, vol. 11, pp. 113–150.
83 M. Al-Amin, A. M. Abdul-Rani, M. Danish, S. Rubaiee, A. B. Mahfouz, H. M. Thompson, S. Ali, D. R. Unune and M. H. Sulaiman, *Materials*, 2021, **14**, 3597.
84 P. Piljek, Z. Keran and M. Math, *Interdiscip. Descr. Complex Syst.*, 2014, **12**, 1–27.
85 S. Ge-Zhang, H. Yang, H. Ni, H. Mu and M. Zhang, *Front. Bioeng. Biotechnol.*, 2022, **10**, 958095.
86 M. J. Moreno-Lizaranzu and F. Cuesta, *Sensors*, 2013, **13**, 13521–13542.
87 Y. X. Kato, S. Furukawa, K. Samejima, N. Hironaka and M. Kashino, *Front. Neuroeng.*, 2012, **5**, 11.
88 H. Becker and C. Gaertner, *Rev. Mol. Biotechnol.*, 2001, **82**, 89–99.
89 M. V. Kothare, *Comput. Chem. Eng.*, 2006, **30**, 1725–1734.
90 P. L. Suryawanshi, S. P. Gumfekar, P. R. Kumar, B. B. Kale and S. H. Sonawane, *Colloid Interface Sci. Commun.*, 2016, **13**, 6–9.
91 M. Rašljić Rafajilović, K. Radulović, M. M. Smiljanić, Ž. Lazić, Z. Jakšić, D. Stanisavljev and D. V. Radović, *Micromachines*, 2020, **11**, 818.
92 S. N. Yusoh and K. A. Yaacob, *Beilstein J. Nanotechnol.*, 2016, **7**, 1461–1470.
93 X.-f Hu, C.-g Lu, Q. Wang, J.-k Xu and Y.-p Cui, *RSC Adv.*, 2020, **10**, 38220–38226.
94 P. L. Urban, D. M. Goodall and N. C. Bruce, *Biotechnol. Adv.*, 2006, **24**, 42–57.
95 D. A. Waterkamp, M. Heiland, M. Schlüter, J. C. Sauvageau, T. Beyersdorff and J. Thöming, *Green Chem.*, 2007, **9**, 1084–1090.
96 D. Kulkarni, F. Damiri, S. Rojekar, M. Zehravi, S. Ramproshad, D. Dhoke, S. Musale, A. A. Mulani, P. Modak and R. Paradhi, *Pharmaceutics*, 2022, **14**, 1097.
97 H. Schröder, E. Obermeier and A. Steckenborn, *J. Micromech. Microeng.*, 1999, **9**, 139.
98 L. Wu, L. Cui, W. He, J. Guo, B. Yu and L. Qian, *ACS Appl. Mater. Interfaces*, 2022, **14**, 29366–29376.
99 A. Rietig, T. Langner and J. Acker, *Phys. Chem. Chem. Phys.*, 2019, **21**, 22002–22013.
100 M. Bauhuber, A. Mikrievskij and A. Lechner, *Mater. Sci. Semicond. Process.*, 2013, **16**, 1428–1433.
101 A. Woitalka, S. Kuhn and K. F. Jensen, *Chem. Eng. Sci.*, 2014, **116**, 1–8.
102 S. Odiba, M. Olea, T. Sasaki, E. Iro, S. Hodgson, A. Adgar and P. Russell, *Catalysts*, 2020, **10**, 846.
103 C.-W. Wang, A. Bains, D. Sinton and M. G. Moffitt, *Langmuir*, 2013, **29**, 8385–8394.
104 A.-G. Niculescu, D. E. Mihaiescu and A. M. Grumezescu, *Int. J. Mol. Sci.*, 2022, **23**, 8293.
105 B. Sun, H. Zhu, W. Liang, X. Zhang, J. Feng and W. Xu, *Int. J. Hepatol.*, 2019, **44**, 19547–19554.
106 L. Lin and C.-K. Chung, *Micromachines*, 2021, **12**, 1350.
107 Z. Li, X. Zu, Z. Du and Z. Hu, *Sci. Rep.*, 2021, **11**, 19995.
108 K. Osouli-Bostanabad, S. Puliga, D. R. Serrano, A. Bucchi, G. Halbert and A. Lalatsa, *Pharmaceutics*, 2022, **14**, 1940.
109 J. Zhang, T. Zheng, L. Tang, H. Qi, X. Wu and L. Zhu, *Micromachines*, 2022, **13**, 1337.
110 Y. Wang, S. Rink, A. J. Baeumner and M. Seidel, *Microchim. Acta*, 2022, **189**, 117.
111 W. Guo, L. Tang, B. Zhou and Y. Fung, *Micromachines*, 2021, **12**, 153.
112 F. Mahmud, K. F. Tamrin, S. Mohamaddan and N. Watanabe, *Processes*, 2021, **9**, 891.
113 S. Shyam, P. K. Mondal and B. Mehta, *J. Fiz. Malays.*, 2021, **917**, A15.
114 J. Lee, S. Lee, M. Lee, R. Prakash, H. Kim, G. Cho and J. Lee, *Micromachines*, 2022, **13**, 1218.
115 G. Singh, BAPS, 2023.
116 Z. Li, B. Zhang, D. Dang, X. Yang, W. Yang and W. Liang, *Sens. Actuators, A*, 2022, 113757.
117 R. H. Liu, M. A. Stremler, K. V. Sharp, M. G. Olsen, J. G. Santiago, R. J. Adrian, H. Aref and D. J. Beebe, *J. Microelectromech. Syst.*, 2000, **9**, 190–197.
118 L.-R. Huang, L.-L. Fan, Q. Liu, Z. Zhao, J. Zhe and L. Zhao, *J. Micromech. Microeng.*, 2021, **31**, 055009.
119 A. D. Stroock, S. K. Dertinger, A. Ajdari, I. Mezic, H. A. Stone and G. M. Whitesides, *Science*, 2002, **295**, 647–651.
120 J. Wang, J. A. Apresa, M. Weathered, A. Perez and M. Corradini, *Int. J. Hydrogen Energy*, 2021, **46**, 38887–38902.
121 C. Matthews, V. Laboure, M. DeHart, J. Hansel, D. Andrs, Y. Wang, J. Ortensi and R. C. Martineau, *Nucl. Technol.*, 2021, **207**, 1142–1162.
122 P. Sabharwall, J. Gibb, C. Ritter, K. Araújo, A. Gupta, I. Ferguson, B. Rolston, R. Fisher, J. Gehin and Y. Ballout, *Cyber Secur.: A Peer-Rev. J.*, 2021, **4**, 345–367.
123 J. H. Ferziger, M. Perić and R. L. Street, *Computational methods for fluid dynamics*, Springer, Berlin, 2002.
124 Y. Fujii, K. Imagawa, T. Omura, T. Suzuki and H. Minami, *ACS Omega*, 2020, **5**, 1919–1926.
125 P. Saha, M. Mahiuddin, A. N. Islam and B. Ochiai, *ACS Omega*, 2021, **6**, 18260–18268.
126 T. M. Tolaymat, A. M. El Badawy, A. Genaidy, K. G. Scheckel, T. P. Luxton and M. Suidan, *Sci. Total Environ.*, 2010, **408**, 999–1006.
127 J. Wagner, T. Kirner, G. Mayer, J. Albert and J. Köhler, *Chem. Eng. J.*, 2004, **101**, 251–260.
128 J. Wagner and J. Köhler, *Nano Lett.*, 2005, **5**, 685–691.
129 J. Wagner, T. Tshikhudo and J. Köhler, *Chem. Eng. J.*, 2008, **135**, S104–S109.
130 L. Panariello, S. Damilos, H. du Toit, G. Wu, A. N. Radhakrishnan, I. P. Parkin and A. Gavriilidis, *React. Chem. Eng.*, 2020, **5**, 663–676.
131 H. Van Nguyen, H. Van Nguyen, V. M. Phan, B. J. Park and T. S. Seo, *Chem. Eng. J.*, 2023, **452**, 139044.
132 X. Zhang, S. Ma, A. Li, L. Chen, J. Lu, X. Geng, M. Xie, X. Liang, Y. Wan and P. Yang, *Appl. Nanosci.*, 2020, **10**, 661–669.
133 M. A. Abdel-Lateef, *Sci. Rep.*, 2022, **12**, 6953.
134 J. A. Badán, E. Navarrete-Astorga, R. Henríquez, F. M. Jiménez, D. Ariosa, J. R. Ramos-Barrado and E. A. Dalchiele, *Nanomaterials*, 2022, **12**, 617.

135 C. Faure, A. Derré and W. Neri, *J. Phys. Chem. B*, 2003, **107**, 4738–4746.
136 A. Nightingale, S. Krishnadasan, D. Berhanu, X. Niu, C. Drury, R. McIntyre, E. Valsami-Jones and J. DeMello, *Lab Chip*, 2011, **11**, 1221–1227.
137 R. M. N. Lintag, F. G. D. Leyson, M. S. B. Matibag and K. J. R. Yap, *Mater. Today: Proc.*, 2020, **22**, 185–192.
138 M. Wojnicki, T. Tokarski, V. Hessel, K. Fitzner and M. Luty-Błocho, *Chem. Eng. J.*, 2020, **382**, 122922.
139 J. Baumgard, A.-M. Vogt, U. Kragl, K. Jähnisch and N. Steinfeldt, *Chem. Eng. J.*, 2013, **227**, 137–144.
140 L. Xu, J. Peng, C. Srinivasakannan, L. Zhang, D. Zhang, C. Liu, S. Wang and A. Q. Shen, *RSC Adv.*, 2014, **4**, 25155–25159.
141 L. Xu, J. Peng, C. Srinivasakannan, G. Chen and A. Q. Shen, *Appl. Surf. Sci.*, 2015, **355**, 1–6.
142 L. Xu, C. Srinivasakannan, J. Peng, D. Zhang and G. Chen, *Chem. Eng. Process.*, 2015, **93**, 44–49.
143 W. Zhang, P. Zhang, D. Lu, H. Pan, X. Liu, C. Xu, J. Wei, M. Li and H. Ji, *J. Mater. Sci. Technol.*, 2023, **145**, 56–65.
144 Y. Zhong, X. T. Zheng, Q.-L. Li, X. J. Loh, X. Su and S. Zhao, *Biosens. Bioelectron.*, 2023, **224**, 115033.
145 Y. Ren, W. Zheng, S. Li and Y. Liu, *J. Hazard. Mater.*, 2023, **445**, 130520.
146 J. S. Santana, K. M. Koczkur and S. E. Skrabalak, *React. Chem. Eng.*, 2018, **3**, 437–441.
147 S. Cattaneo, S. Althahban, S. J. Freakley, M. Sankar, T. Davies, Q. He, N. Dimitratos, C. J. Kiely and G. J. Hutchings, *Nanoscale*, 2019, **11**, 8247–8259.
148 H. Liu, J. Huang, D. Sun, T. Odoom-Wubah, J. Li and Q. Li, *J. Nanopart. Res.*, 2014, **16**, 1–9.
149 C. Zeng, C. Wang, F. Wang, Y. Zhang and L. Zhang, *Chem. Eng. J.*, 2012, **204**, 48–53.
150 Y. Song, C. S. Kumar and J. Y. Hormes, *J. Nanosci. Nanotechnol.*, 2004, **4**, 788–793.
151 E. Gioria, F. Wisniewski and L. Gutierrez, *J. Environ. Chem. Eng.*, 2019, **7**, 103136.
152 M. Yang, L. Luo and G. Chen, *AIChE J.*, 2020, **66**, e16950.
153 K. C. Chou and X. M. Hou, *J. Am. Ceram. Soc.*, 2009, **92**, 585–594.
154 M. Di Mare and C. M. Ouellet-Plamondon, *J. Sustainable Metall.*, 2022, 1–6.
155 H. Pang, C. Bourgès, R. Jha, T. Baba, N. Sato, N. Kawamoto, T. Baba, N. Tsujii and T. Mori, *Acta Mater.*, 2022, **235**, 118090.
156 Y. Fu, H. Zhu, J. Chen, M. P. Hautzinger, X.-Y. Zhu and S. Jin, *Nat. Rev. Mater.*, 2019, **4**, 169–188.
157 F. P. García de Arquer, D. V. Talapin, V. I. Klimov, Y. Arakawa, M. Bayer and E. H. Sargent, *Science*, 2021, **373**, eaaz8541.
158 H. Qiao, H. Liu, Z. Huang, R. Hu, Q. Ma, J. Zhong and X. Qi, *Energy Environ. Mater.*, 2021, **4**, 522–543.
159 L. Pitkänen and A. M. Striegel, *TrAC, Trends Anal. Chem.*, 2016, **80**, 311–320.
160 R. Priyadarshi, P. Ezati and J.-W. Rhim, *Environ. Chem. Lett.*, 2022, 1–16.
161 J. B. Edel, R. Fortt, J. C. de Mello and A. J. de Mello, *Controlled Quantum Dot Synthesis within Microfluidic Circuits*, Springer, Netherlands, Dordrecht, 2002, pp. 772–774.
162 R. Kikkeri, P. Laurino, A. Odedra and P. H. Seeberger, *Angew. Chem., Int. Ed.*, 2010, **49**, 2054–2057.
163 L. Rao, Y. Tang, H. Lu, S. Yu, X. Ding, K. Xu, Z. Li and J. Z. Zhang, *Nanomaterials*, 2018, **8**, 900.
164 A. Hebbar, R. Selvaraj, R. Vinayagam, T. Varadavenkatesan, P. S. Kumar, P. A. Duc and G. Rangasamy, *Chemosphere*, 2022, 137308.
165 M. A. Green, A. Ho-Baillie and H. J. Snaith, *Nat. Photonics*, 2014, **8**, 506–514.
166 A. Ren, H. Wang, W. Zhang, J. Wu, Z. Wang, R. V. Penty and I. H. White, *Nat. Electron.*, 2021, **4**, 559–572.
167 M. Ye, G. M. Biesold, M. Zhang, W. Wang, T. Bai and Z. Lin, *Nano Today*, 2021, **40**, 101286.
168 W. Travis, E. Glover, H. Bronstein, D. Scanlon and R. Palgrave, *Chem. Sci.*, 2016, **7**, 4548–4556.
169 H. A. Evans, Y. Wu, R. Seshadri and A. K. Cheetham, *Nat. Rev. Mater.*, 2020, **5**, 196–213.
170 S.-M. Kang, B. Park, G. S. R. Raju, S. Baek, S. K. Hussain, C. H. Kwak, Y.-K. Han, J. S. Yu, S.-W. Kim and Y. S. Huh, *Chem. Eng. J.*, 2020, **384**, 123316.
171 Y. Geng, J. Guo, S. D. Ling, X. Wu, H. Liu, Z. Chen, S. Chen and J. Xu, *Sci. China Mater.*, 2022, **65**, 2746–2754.
172 Y. Geng, J. Guo, H. Wang, S. D. Ling, Z. Chen, S. Chen and J. Xu, *Small*, 2022, **18**, 2200740.
173 T.-H. Shin, Y. Choi, S. Kim and J. Cheon, *Chem. Soc. Rev.*, 2015, **44**, 4501–4516.
174 G. Chen, B. Yu, C. Lu, H. Zhang, Y. Shen and H. Cong, *CrystEngComm*, 2018, **20**, 7486–7491.
175 L. Zou, B. Huang, X. Zheng, H. Pan, Q. Zhang, W. Xie, Z. Zhao and X. Li, *Mater. Chem. Phys.*, 2022, **276**, 125384.
176 F. W. Ling, H. A. Abdulbari and S.-Y. Chin, *Mater. Today: Proc.*, 2021, **42**, 1–7.
177 F. W. Ling, H. A. Abdulbari and C. Sim-Yee, *J. Flow Chem.*, 2022, **12**, 17–30.
178 N. Kockmann, J. Kastner and P. Woias, *Chem. Eng. J.*, 2008, **135**, S110–S116.
179 Q.-A. Wang, J.-X. Wang, M. Li, L. Shao, J.-F. Chen, L. Gu and Y.-T. An, *Chem. Eng. J.*, 2009, **149**, 473–478.
180 L. Du, Y. Wang, Y. Lu and G. Luo, *Powder Technol.*, 2013, **247**, 60–68.
181 H. Yang, S. X. Wei, H. Chen, L. Chen, C. T. Au, T. L. Xie and S. F. Yin, *AIChE J.*, 2022, **68**, e17810.
182 H. Wang, H. Nakamura, M. Uehara, M. Miyazaki and H. Maeda, *Chem. Commun.*, 2002, 1462–1463.
183 M. Takagi, T. Maki, M. Miyahara and K. Mae, *Chem. Eng. J.*, 2004, **101**, 269–276.
184 S. Appalakutti, S. Sonawane, B. A. Bhanvase, V. Mittal and M. Ashokkumar, *Chem. Eng. Process.*, 2015, **89**, 28–34.
185 H. Nakamura, Y. Yamaguchi, M. Miyazaki, M. Uehara, H. Maeda and P. Mulvaney, *Chem. Lett.*, 2002, 1072–1073.
186 E. M. Chan, R. A. Mathies and A. P. Alivisatos, *Nano Lett.*, 2003, **3**, 199–201.

187 J. Hiemer, A. Clausing, T. Schwarz and K. Stöwe, *Chem. Eng. Technol.*, 2019, **42**, 2018–2027.
188 Y.-F. Su, H. Kim, S. Kovenklioglu and W. Lee, *J. Solid State Chem.*, 2007, **180**, 2625–2629.
189 D. Jeevarathinam, A. Gupta, B. Pitchumani and R. Mohan, *Chem. Eng. J.*, 2011, **173**, 607–611.
190 C. Delacour, C. Lutz and S. Kuhn, *Ultrason. Sonochem.*, 2019, **55**, 67–74.
191 C. Chung, T. Shih, C. Chang, C. Lai and B. Wu, *Chem. Eng. J.*, 2011, **168**, 790–798.
192 B. Palanisamy and B. Paul, *Chem. Eng. Sci.*, 2012, **78**, 46–52.
193 Y. Chen, M. Alba, T. Tieu, Z. Tong, R. S. Minhas, D. Rudd, N. H. Voelcker, A. Cifuentes-Rius and R. Elnathan, *Adv. NanoBiomed Res.*, 2021, **1**, 2100002.
194 G. Zhou, E. Goshi and Q. He, *Adv. Healthcare Mater.*, 2019, **8**, 1900463.
195 Q. Zhao, H. Cui, Y. Wang and X. Du, *Small*, 2020, **16**, 1903798.
196 V. Hakke, S. Sonawane, S. Anandan, S. Sonawane and M. Ashokkumar, *Nanomaterials*, 2021, **11**, 98.
197 R. A. Petros and J. M. DeSimone, *Nat. Rev. Drug Discovery*, 2010, **9**, 615–627.
198 A. D. Bangham, M. M. Standish and J. C. Watkins, *J. Mol. Biol.*, 1965, **13**, 238.
199 K. Kuribayashi, G. Tresset, P. Coquet, H. Fujita and S. Takeuchi, *Meas. Sci. Technol.*, 2006, **17**, 3121.
200 R. Ushiyama, K. Koiwai and H. Suzuki, *Sens. Actuators, B*, 2022, **355**, 131281.
201 I. O. de Solorzano, G. Mendoza, M. Arruebo and V. Sebastian, *Colloids Surf., B*, 2020, **190**, 110904.
202 S. Kim, H. Wang, L. Yan, X. Zhang and Y. Cheng, *Chem. Eng. J.*, 2020, **393**, 124721.
203 S. Maity, T. Bhuyan, R. Bhattacharya and D. Bandyopadhyay, *ACS Appl. Mater. Interfaces*, 2021, **13**, 19430–19442.
204 T. Jaouhari, F. Zhang, T. Tassaing, S. Fery-Forgues, C. Aymonier, S. Marre and A. Erriguible, *Chem. Eng. J.*, 2020, **397**, 125333.
205 J.-i Yoshida, *Chem. Commun.*, 2005, 4509–4516.
206 J. i Yoshida, A. Nagaki and T. Yamada, *Chem. – Eur. J.*, 2008, **14**, 7450–7459.
207 Y. Guo, C. Yang, S. Zhou, Z. Liu and X. Guo, *Adv. Mater.*, 2022, **34**, 2204827.
208 S. Ghinato, F. De Nardi, P. Bolzoni, A. Antenucci, M. Blangetti and C. Prandi, *Chem. – Eur. J.*, 2022, **28**, e202201154.
209 K. Pérez, S. Leveneur, F. Burel, J. Legros and D. Vuluga, *React. Chem. Eng.*, 2023, **8**, 432–441.
210 D. Polterauer, D. M. Roberge, P. Hanselmann, P. Elsner, C. A. Hone and C. O. Kappe, *React. Chem. Eng.*, 2021, **6**, 2253–2258.
211 X. Chen, L. Hou, Z. Yin, K. Wang, Z. Zhang and F. Bao, *Chem. Eng. J.*, 2023, **454**, 140050.
212 W. Yang, X. Tang, W. Li, X. Luo, C. Zhang and C. Shen, *Chem. Eng. J.*, 2022, **442**, 136110.
213 R. Xu, Q. Song, C. Li, J. Li, H. Yang, J. Chen and Z. Mao, *Can. J. Chem. Eng.*, 2022, 1–8.
214 N. Joshi and A. Lawal, *Chem. Eng. Sci.*, 2012, **84**, 761–771.
215 U. Neuenschwander and K. F. Jensen, *Ind. Eng. Chem. Res.*, 2014, **53**, 601–608.
216 Q. Chen, S. Xia, G. Luo and Y. Wang, *Chem. Eng. Sci.*, 2022, **254**, 117645.
217 Y. Jiang and H. Yorimitsu, *JACS Au*, 2022, **2**, 2514–2521.
218 S. Guo, G. Zhu, L. Zhan and B. Li, *Chem. Eng. Res. Des.*, 2022, **178**, 179–188.
219 N. Wang, Y. Jin, T. Huang, J. Zhou, Y. Zhang and N. Li, *J. Taiwan Inst. Chem. Eng.*, 2022, **138**, 104465.
220 T. Tongtummachat, A. Jaree and N. Akkarawatkhoosith, *RSC Adv.*, 2022, **12**, 23366–23378.
221 W. Guo, H. C. Bruining, H. J. Heeres and J. Yue, *AIChE J.*, 2022, **68**, e17606.
222 D. Stradomska, J. Coloma, U. Hanefeld and K. Szymańska, *Catal. Sci. Technol.*, 2022, **12**, 3356–3362.
223 M. Yuan, H. Feng, W. Zhang, J. Zheng, K. Zhang, X. Kong, N. Han and J. Dong, *Chem. Eng. Process.*, 2022, **174**, 108890.
224 Q. Chen, S. Xia, Y. Wang, G. Luo, H. Shang and K. Wang, *AIChE J.*, 2021, **67**, e17217.
225 A. Yang, X. Yang, J. Yue, S. Zheng and L. Qin, *Chem. Eng. Technol.*, 2022, **45**, 6–14.
226 Z. Yang, Y. Yang, X. Zhang, W. Du, J. Zhang, G. Qian, X. Duan and X. Zhou, *AIChE J.*, 2022, **68**, e17498.
227 N. Sen, K. Singh, S. Mukhopadhyay and K. Shenoy, *Chem. Eng. Process.*, 2021, **166**, 108431.
228 W. Sailer-Kronlachner, C. Thoma, S. Böhmdorfer, M. Bacher, J. Konnerth, T. Rosenau, A. Potthast, P. Solt and H. W. Van Herwijnen, *ACS omega*, 2021, **6**, 16641–16648.
229 Y. Xie, Q. Chen, G. Huang, Y. Wang, W. Hu, Z. Yan, X. Wang, J. Huang, M. Gao and W. Fei, *AIChE J.*, 2021, **67**, e17231.
230 H. Khorshidi, C. Zhang, E. Najafi and M. Ghasemi, *J. Cleaner Prod.*, 2022, 135390.
231 T. Mai, D.-D. Li, L. Chen and M.-G. Ma, *Carbohydr. Polym.*, 2022, 120359.
232 Z. Liu, D. J. McClements, A. Shi, L. Zhi, Y. Tian, B. Jiao, H. Liu and Q. Wang, *Crit. Rev. Food Sci. Nutr.*, 2022, 1–12.
233 G. Wang, S. Jia, H. Gao, Y. Shui, J. Fan, Y. Zhao, L. Li, W. Kang, N. Deng and B. Cheng, *J. Energy Chem.*, 2023, **76**, 377–397.
234 X. Wang, L. Wang, D. Wu, D. Yuan, H. Ge and X. Wu, *Sci. Total Environ.*, 2022, 158880.
235 Y. Zhang, K. Yang, R. Liu, J. Yao and H. Yan, *Chem. Eng. J.*, 2023, 141773.
236 P.-G. De Gennes, *Science*, 1992, **256**, 495–497.
237 P. G. de Gennes, *Angew. Chem., Int. Ed. Engl.*, 1992, **31**, 842–845.
238 Q. Bai, I. Shupyk, L. Vauriot, J. Majimel, C. Labrugere, M.-H. Delville and J.-P. Delville, *ACS Nano*, 2021, **15**, 2947–2961.
239 A. Dobhal, A. Srivastav, P. Dandekar and R. Jain, *J. Mater. Sci.: Mater. Med.*, 2021, **32**, 1–18.
240 G. Tofighi, H. Lichtenberg, A. Gaur, W. Wang, S. Wild, K. H. Delgado, S. Pitter, R. Dittmeyer, J.-D. Grunwaldt and D. E. Doronkin, *React. Chem. Eng.*, 2022, **7**, 730–740.
241 Y. Chai, Y. Wang, B. Li, W. Qi, R. Su and Z. He, *Langmuir*, 2021, **37**, 7219–7226.

242 C. Li, Q. Liu and S. Tao, *Nat. Commun.*, 2022, **13**, 6034.
243 L. Xu, J. Peng, B. Meng, W. Li, B. Liu and H. Luo, *High Temp. Mater. Processes*, 2016, **35**, 745–750.
244 L. Xu, C. Srinivasakannan, J. Peng, M. Yan, D. Zhang and L. Zhang, *Appl. Surf. Sci.*, 2015, **331**, 449–454.
245 L. Xu, C. Srinivasakannan, J. Peng, L. Zhang and D. Zhang, *J. Alloys Compd.*, 2017, **695**, 263–269.
246 M. Kaur, M. Yusuf, Y. F. Tsang, K.-H. Kim and A. K. Malik, *Sci. Total Environ.*, 2023, **857**, 159385.
247 B. E. Snyder, A. B. Turkiewicz, H. Furukawa, M. V. Paley, E. O. Velasquez, M. N. Dods and J. R. Long, *Nature*, 2023, **613**, 287–291.
248 Y. Xu, A. K. Rashwan, A. I. Osman, E. M. Abd El-Monaem, A. M. Elgarahy, A. S. Eltaweil, M. Omar, Y. Li, A.-H. E. Mehanni and W. Chen, *Environ. Chem. Lett.*, 2022, 1–31.
249 M. Faustini, J. Kim, G.-Y. Jeong, J. Y. Kim, H. R. Moon, W.-S. Ahn and D.-P. Kim, *J. Am. Chem. Soc.*, 2013, **135**, 14619–14626.
250 J. Chen, Z. Zhu, G. Monge and W.-N. Wang, *Chem. Eng. J.*, 2022, **447**, 137544.
251 A. Fujiwara, S. Watanabe and M. T. Miyahara, *Langmuir*, 2021, **37**, 3858–3867.
252 N. A. Jose, J. J. Varghese, S. H. Mushrif, H. C. Zeng and A. A. Lapkin, *J. Phys. Chem. C*, 2021, **125**, 22837–22847.
253 N. A. Jose, H. C. Zeng and A. A. Lapkin, *Chem. Eng. J.*, 2020, **388**, 124133.
254 H. Wang, X. Li, M. Uehara, Y. Yamaguchi, H. Nakamura, M. Miyazaki, H. Shimizu and H. Maeda, *Chem. Commun.*, 2004, 48–49.
255 S. Tai, W. Zhang, J. Zhang, G. Luo, Y. Jia, M. Deng and Y. Ling, *Microporous Mesoporous Mater.*, 2016, **220**, 148–154.
256 S. Watanabe, S. Ohsaki, T. Hanafusa, K. Takada, H. Tanaka, K. Mae and M. T. Miyahara, *Chem. Eng. J.*, 2017, **313**, 724–733.
257 T. Didriksen, A. I. Spjelkavik and R. Blom, *J. Flow Chem.*, 2017, **7**, 13–17.
258 D. Liu, Y. Jing, K. Wang, Y. Wang and G. Luo, *Nanoscale*, 2019, **11**, 8363–8371.
259 J. Zhang, Y. Wang and F. Wang, *Inorg. Chem. Commun.*, 2019, **109**, 107566.
260 G. Kibar, U. Çalışkan, E. Y. Erdem and B. Çetin, *J. Polym. Sci., Part A: Polym. Chem.*, 2019, **57**, 1396–1403.
261 Y. He, Z. Chen and C.-H. Chang, *Nanotechnol.*, 2020, **31**, 235603.
262 L. Luo, M. Yang and G. Chen, *Chem. Eng. Sci.*, 2022, **251**, 117479.
263 S. Sohrabi, M. K. Moraveji and D. Iranshahi, *Rev. Chem. Eng.*, 2020, **36**, 687–722.
264 Z. Dong, D. F. Rivas and S. Kuhn, *Lab Chip*, 2019, **19**, 316–327.
265 S. Zhao, C. Yao, Z. Dong, Y. Liu, G. Chen and Q. Yuan, *Chem. Eng. Sci.*, 2018, **186**, 122–134.
266 D. A. Cristaldi, F. Yanar, A. Mosayyebi, P. García-Manrique, E. Stulz, D. Carugo and X. Zhang, *New Biotechnol.*, 2018, **47**, 1–7.
267 K. Y. Nandiwale, T. Hart, A. F. Zahrt, A. M. Nambiar, P. T. Mahesh, Y. Mo, M. J. Nieves-Remacha, M. D. Johnson, P. García-Losada and C. Mateos, *React. Chem. Eng.*, 2022, **7**, 1315–1327.
268 I. Merino-Garcia, G. García, I. Hernández and J. Albo, *J. CO2 Util.*, 2023, **67**, 102340.
269 S. Zuo, Y. Ding, L. Wu, F. Yang, Z. Guan, S. Ding, D. Xia, X. Li and D. Li, *Water Res.*, 2023, 119631.

